A bacterial-like mechanosensitive channel controls osmoregulation and infectivity in *Trypanosoma cruzi.*

Dave, N[1]; Cetiner, U[2]; Arroyo, D[1]; Fonbuena, J[1]; Barrera, P[3]; Lander, N[4]; Anishkin, A[2]; Sukharev, S[2] and Jimenez, V[1]*

[1]Department of Biological Science, College of Natural Sciences and Mathematics, California State University Fullerton; [2]Department of Biology, University of Maryland, College Park; [3] Departmento de Biología, Facultad de Ciencias Exactas y Naturales, Instituto de Histologia y Embriologia IHEM-CONICET, Facultad de Medicina, Universidad Nacional de Cuyo ; [4]Center for Tropical and Emerging Global Diseases, University of Georgia, Athens, GA.

Running title: A mechanosensitive channel in *Trypanosoma cruzi*

Address: [1]Department of Biological Sciences, College of Natural Sciences and Mathematics, California State University Fullerton. 800 N State College Blvd, McCarthy Hall 307, Fullerton, California 92831, U.S.A. Tel: 1-657-278-2477, Fax: 1-657-278-5390

e-mail: vjimenezortiz@fullerton.edu. *Correspondence and reprints.

Keywords: mechanosensation, osmoregulation, infectivity, CRISPR-Cas9, electrophysiology.

Abstract

Trypanosoma cruzi, the causative agent of Chagas disease undergoes drastic cellular morphological and biochemical changes as it passes from extracellular epimastigote and trypomastigote forms, to intracellular/tissue non-motile stage. Here we describe and characterize a mechanosensitive channel in *T. cruzi* (TcMscS), which is homologous to bacterial MscS. TcMscS is present in the contractile vacuole of extracellular stages but redistributes to the plasma membrane in intracellular amastigotes. The heterologously expressed TcMscS is activated by membrane tension (12 mN/m) forming a large 0.4 nS pore permeable to both anions and cations and possibly small osmolytes. The TcMscS knockdown and knockout *T. cruzi* strains, generated by CRISPR-Cas9 gene targeting, show slower growth in intracellular and extracellular stages, inability to robustly regulate volume and a dramatically decreased infectivity. Our study shows that the tension-driven mechanosensitive channel fulfills multiple roles in different stages of *T. cruzi* life cycle and is essential for infectivity.

Significance

Protozoan parasites transmited by insect vectors have the ability to infect a variety of mammalian host, completing their development in various environments. Their capacity to detect and respond to changes in external conditions is key for their survival but the mechanisms involved in sensing are poorly described. Mechanosensation plays an important role in regulating pathogenicity and cell development. Here, we have identified and characterized a mechanosensitive channel required for osmotic regulation in *Trypanosoma cruzi*. The ablation of the gene renders parasites with impaired replication and severe infectivity defects. Our work is providing new elements to understand host-pathogen interaction and cellular homeostasis.

Introduction

Several protozoan pathogens complete their life cycle alternating between mammalian hosts and insect vectors (1-3) with periods of exposure to the environment. *Trypanosoma cruzi*, a flagellated protozoan is the causative agent of Chagas disease, an endemic pathology in Latin America where millions are infected (4). Recent studies in the epidemiology of the disease show an increased incidence in non-endemic regions of the world (5, 6). In its intricate life cycle, the parasite undergoes transitions between intracellular and free-living forms, which involve drastic morphological and biochemical changes that ensure survival in different environments. Understanding intracellular compartments, physical factors and molecules that impart mechanical and osmotic stability to the cell during these transitions may increase.

T. cruzi completes its life cycle by by alternating between mammalian hosts and insect vectors (1). Motile epimastigotes replicate in the intestinal lumen of the insect vector, enduring the concentration of the rectal content up to 1000 mOsm/Kg (7). After differentiating into metacyclic trypomastigotes, the parasites are released to the environment in the feces of the vector, penetrate the skin layers of a mammalian host and disseminate through the circulation. The flagellated and highly motile trypomastigotes survive shear stress in the bloodstream and penetrate into the cells where they transform to the stage of round non-motile intracellular amastigotes, which proliferate in a relatively constant cytosolic environment. The differentiation back to the infective and extracellular trypomastigotes requires substantial volume and shape changes, cytoskeletal rearrangement and generation if the free flagella.

To regulate volume, *T. cruzi* and other protozoans have robust compensatory mechanisms based on the activity of the contractile vacuole complex (CVC) (8, 9). The CVC is a bipartite specialized organelle formed by a bladder and a network of tubular vesicles called spongiome (10). It is present in protozoans, including *Paramecium, Dictyostelium and Chlamydomonas* (11). In *T. cruzi* the CVC is involved in the regulation of cell volume (8),

calcium homeostasis and protein trafficking (12). Despite the description of numerous proteins, including aquaporins (13) involved in the function of the CVC in *T. cruzi*, the precise mechanisms by which trypanosomatids are able to detect changes and respond to changes in external conditions are not clear. Osmotic responses, invasion and differentiation (14-16) involve an important mechanical component that must be detected, but the mechanosensors coordinating these processes and especially molecules that detect and respond to stress in the membrane are yet to be identified.

Mechanosensation is a universal characteristic of all organisms, from bacteria to mammals (17, 18). It allows cells to respond to stress conditions, maintaining relatively constant volume and macromolecular composition of the cytoplasm. Failure to compensate osmotic changes may result in cell death either by swelling and bursting, or by activation of apoptotic mechanisms under persistent hyperosmotic stress (19).

Beyond osmoregulation, in eukaryotic organisms mechanosensation is involved in shear stress sensing via transient receptor potential (TRP) (20, 21) and Piezo channel activation (22). In prokaryotes, MS channels have been suggested to participate in quorum sensing, biofilm formation and regulation of virulence factors (23, 24, 25). In bacteria, large- conductance (MscL) (26) and small-conductance mechanosensitive channels (MscS) (27) have been defined as key players in osmotic regulation, acting as valves to release osmolytes upon hyposmotic shock (28). McsS-like channels have been found in Archaea (29), fungi (30), protozoans (31, 32) and plants (33). They belong to the MscS family, but have evolved and diversified in structure and function, playing roles in osmoregulation, Ca^{2+} homeostasis, and organelle biogenesis and maintenance (34-37).

In *T. cruzi,* bioinformatic analysis revealed the presence of several putative MS channels with sequence similarity to bacterial-like MS and Piezo channels (38). We hypothesize that MS channels in *T. cruzi* might be involved in sensing fluid shear stress and mechanical tension generated during tissue migration and cell penetration. Additionally, MscS-like channels could

play a role in ion and osmolyte fluxes required for volume regulation. Here, we report the identification and functional characterization of a mechanosensitive channel from the MscS family present in *T. cruzi* (TcMscS). The channel expressed in bacterial spheroplasts shows gating by membrane tension, without requiring additional elements for its activation. In the parasites, the channel resides in the CV complex of extracellular stages, and translocates to the plasma membrane in intracellular amastigotes. Gene targeting by CRISPR/Cas methods renders knockout and knockdown parasites with impaired growth and inability to robustly regulate cell volume. We also observed a dramatic decrease in infectivity supporting the essential role of tension-driven mechanosensitive channels in *T. cruzi* life cycle.

Results

Sequence analysis and structural features of TcMscS predicted by homology model

Analysis of Trypanosoma databases (tritrypdb.org) revealed the presence of a putative MscS-like ion channel (TcCLB.504171.40) in the Esmeraldo-like haplotype of the *T. cruzi* CL Brener strain genome (TcMscS). This channel shares 94.5% identity, at protein level, with the non Esmeraldo-like allele (TcCLB.509795.40) and has homologues in *T. brucei* (Tb427.10.9030) and *Leishmania major* (LmjF.36.5770), sharing 66% and 58% identity, respectively (Fig. 1A). Overall sequence conservation between TcMscS and *E. coli* MscS is low (25.4%), but the percentage of identity increases to 38% in the core comprising transmembrane helices TM2 and TM3.

The ORF of TcMscS is 498 nucleotides, predicting a protein of 165 amino acids with apparent molecular weight of 17.8 kDa. Assuming that TcMscS follows the same oligomerization pattern as *E. coli* MscS (39), it is expected to form a heptamer. The refined consensus homology model based on several structure prediction servers (Fig. 1B) indicates the presence of 2 transmembrane domains, with a preceding N-terminal segment (red). The chain continues as TM2 (gold), crosses the membrane, makes a short loop and returns back as pore-forming TM3

(green). The gate of TcMscS is predicted to be formed by the ring of F64 which is in the precise homologous position with the gate-forming L109 of EcMscS.

The labeling of TcMscS helices in Fig. 1 matches the homologous segments of prokaryotic MscS channels. Because the TM1 segment in TcMscS is too short to assume a transmembrane position, it is modeled in the conformation attached to the inner surface of the membrane. The beta domain (cyan) is the last segment that aligns with EcMscS. The full alignment of four protozoan and two bacterial sequences is shown in supplemental Figure S1 and the complete TcMscS homology model, which includes the bundled C-terminal segment is shown on Figure S2. The modeled opening transition shown in the supplemental figure involves an ~3Å outward displacement and tilting of the transmembrane helices. In addition to the F64 constriction (main gate), the beta domain that follows TM3 is predicted to bear a second hydrophobic constriction (Fig. S2 top panel, pink). This hypothetical C-terminal (cytoplasmic) gate formed by L97 (Fig. S2, bottom panel, yellow) is narrower than the cage constriction present in *E. coli* MscS. The *de novo* modeled flexible linkers lead to the C-terminal amphipathic helical domains is hypothesized to form a coiled-coil bundle (blue), similar to what was observed in the crystal structures of MscL, another type of bacterial MS channel. The linkers and bundle might serve as a pre-filter to exclude larger osmolytes from occluding the pore. The full model (Fig. S2) also shows the predicted opening transition which widens the two gates. The overall displacement and tilting of TM3 helices on opening transition is modeled to widen the main gate radius from 3.9 to 6.5 Å accompanied by an in-plane area expansion of the protein by approximately 5.0 nm^2, consistent with the functional gating area estimation presented below.

Electrophysiological characteristics of TcMscS

To evaluate the functional properties of TcMscS, electrophysiological recordings were performed in spheroplasts expressing the channel. Single-channel currents were measured at

low protein expression, with 1-3 channels per patch. Fig. 2A shows typical single-channel traces recorded under 110 mmHg pressure steps at +40 and -40 mV pipette voltages. The current amplitude of 12 pA, translates into the 0.40±0.02 nS conductance (n=11). The I-V curve for TcMscS obtained under symmetric electrolyte conditions is linear (Fig 2B, black symbols), in contrast to EcMscS, which shows a visible rectification (lower conductance at negative pipette voltages) (27, 40). After a perfusion of buffer containing 425 mM KCl in the bath (Fig 2B, red symbols), the I-V curve changes its slope and the x-intercept reproducibly shifts to -4.3 ±0.4mV (n=4). According to Goldman equation, under a given ionic gradient the reversal potential of -4.3 mV corresponds to P_{Cl-}/P_{K+} of 1.6, signifying that the channel passes about 3 Cl^- ions per 2 K^+ ions, i.e. shows a slight anionic preference. Figure 2C-E show two populations recorded at + 30 or -30 mV in the pipette, with identical ramp stimuli. The appearance of channels is essentially identical at two opposite voltages. The channels appear to close slowly as they consistently remain open up to about 10 s after the stimulus ends.

Using pipettes of standard size, we have recorded multiple ramp responses of TcMscS. We then normalized traces to saturating current to find open probability and statistically assessed midpoint pressure required for activation. Using EcMscS as a reference with known tension midpoint, we also estimated the midpoint tension for TcMscS (Fig. 2F). Based on 54 independent patches (recorded with pipettes bubble number of 5.1), EcMscS showed its half-activation pressure at 90±3 mmHg (Fig. 2F, blue symbols). TcMscS, based on 11 patches had its pressure midpoint at 145 ±20 mmHg (Fig. 2F, black symbols). Given that EcMscS activates in *E. coli* spheroplasts at 7.8 mN/m (41), we concluded that the midpoint of TcMscS activation is 12.6 mN/m. Although both channels start opening at approximately the same pressure (tension), the activation curve for TcMscS is shallower. Fitting the initial slopes of logarithmic Po/Pc plots (panel F, inset) using the two-state Boltzmann equation (42) gave estimates of the energies and in-plane area changes associated with gating. Gating of TcMscS was characterized with 3 nm^2 and 7.8 kT, whereas EcMscS curve produced 10.5 nm^2 and 20.4 kT

for the lateral expansion and energy, respectively. The lower area and transition-associated energy for TcMscS are consistent with a 'thinner' protein wall surrounding the aqueous pore and a less hydrophobic pore constriction.

TcMscS channels displayed significant hysteresis during ramp protocols and resisted closing completely even a few seconds after the ramp stimulus ended. Panels 2G and 2H show responses of an 11-channel and 15-channel patches to an asymmetric and symmetric linear ramp of pressure. In both cases, currents do not cease at the end of the ramp and we observed a lingering activity. The channels remain open for a few seconds at zero pressure but 3-7 second after the ramp ends they eventually close. A similar behavior was observed in traces presented in panels 2 C-E.

These results unequivocally demonstrate that TcMscS is a mechanosensitive channel with functional characteristics comparable to the ones observed in bacterial MscS channels. It opens at sub-lytic tensions forming a ~ 12 Å pore, which is essentially non-selective and capable of passing both anions and cations and possibly small organic osmolytes.

TcMscS expression and localization

To determine TcMscS localization, we generated polyclonal antibodies against the recombinant protein. By immunofluorescence analysis (Fig. 3A) we found TcMscS mostly localized in the bladder of the contractile vacuole complex (CVC) of epimastigotes (Fig. 3A) and trypomastigotes (Fig. 3B). The role of CVC as a key regulator of the cell volume in *T. cruzi* has been extensively characterized (8) and the presence of a mechanosensitive channel is consistent with its function in sensing of curbing excessive tension thus protecting the organelle. In epimastigotes, TcMscS colocalizes with VAMP7, another CVC protein (43, 44) (Fig. S3 A) and partially colocalizes with actin (Fig. S3 B) suggesting a possible regulation by interaction with cytoskeleton proteins. Interestingly, no colocalization with tubulin was observed (Fig. S3 C). In trypomastigotes, TcMscS is in the CVC bladder and can also be detected along the flagellum

and the cell body (Fig. 3B) but no co-localization with the membrane marker SSP-1 was observed (Fig. S3 D).

We expressed TcMscS tagged with GFP (Fig. S2 A, B) and confirmed that it also localizes in the CVC (Fig. S2 C). The antibody against TcMscS clearly recognized the native protein at the expected molecular mass of about 17 kDa (Fig. S4 A, E) as well as the overexpressed protein (Fig. S4 A, OE). Parasites overexpressing TcMscS-GFP do not survive beyond a few weeks in culture, and show aberrant morphology, indicating that the activity of the channel must be regulated in order to maintain normal cell functions.

In intracellular amastigotes, TcMscS has a peripheral localization and no evident CVC labeling was detected (Fig. 3C). Colocalization with the amastigote membrane marker SSP-4 shows a clear overlap of the labeling (Fig.S3 E), indicating the translocation of TcMscS to the plasma membrane. The differential localization in the extracellular vs intracellular stages of the parasite suggest that the TcMscS could be playing different physiological roles in response to developmental and/or environmental cues. This hypothesis is reinforced by our data showing that the expression of TcMscS is higher in epimastigotes compared with amastigotes and trypomastigotes, both at mRNA (Fig. 3D) and protein level (Fig. 3E). Epimastigotes at the stationary phase of growth have a significantly lower amount of transcript (Fig. 3D) but no evident difference in the amount of protein was observed by Western blot analysis (data not shown).

One should also consider a simple topological factor: the spherical amastigotes would be more sensitive to osmotic downshock, whereas elongated forms have room for swelling and are better protected by a stronger cytoskeleton, possibly explaining the localization of TcMscS in amastigotes.

TcMscS gene targeting by CRISPR-Cas9

To establish the physiological role of TcMscS in the parasites, we targeted the gene using the CRISPR-Cas9 system with or without DNA donor for gene replacement. When we transfected the parasites with the Cas9/pTREX-n vector containing sgRNA2 (Table S1) targeting *TcMscS,* we observed a single nucleotide deletion (*del*177G), resulting in a shift of the ORF and a premature stop codon (Fig 4A, top panel). These results were confirmed by genomic DNA sequencing in multiple independent samples.

The truncated protein at amino acid 79 is not expected to be functional (Fig 4A, bottom panel), since the C terminal end is absent. In these parasites, the transcript for TcMscS was still detected although at significantly lower level compared with control parasites only expressing Cas9 and a scrambled sgRNA (Fig. 4C). Based on the level of mRNA and the detection of residual protein by Western-blot analysis (Fig. S5, A and B), we considered this strain a knockdown (TcMscS-KD). Importantly, the growth of TcMscS-KD epimastigotes is significantly reduced (Fig. 4B, blue line) when compared to WT (Fig. 4B, black line) and Cas9-scr controls (Fig. 4B, red line). The parasites show abnormal morphology, with rounded bodies and formation of rosettes (Fig. 4D, bottom panel). TcMscS labeling is still present, but the protein is diffusely distributed, probably due to the abnormal folding and trafficking of the truncated channel.

In order to completely abolish the expression of TcMscS, we co-transfected the parasites with sgRNA2-Cas9/pTREX-n vector plus a donor DNA cassette for homologous-directed repair (Fig. 5A). Genomic DNA analysis by PCR shows the absence of *TcMscS* gene, and the correct insertion of the blasticidin resistance cassette (Fig. 5B). No transcript was detected in epimastigotes (Fig. 5D) or trypomastigotes (Fig. S5, C). These results were confirmed by Western blot analysis (Fig. S5, A) and immunofluorescence (Fig. 5E), demonstrating the successful knockout of *TcMscS* (TcMscS-KO).

As expected, the rate of growth of TcMscS-KO epimastigotes was significantly reduced (Fig. 5C, green line), and comparable to the growth of TcMscS-KD parasites (Fig. 5C, blue line). The decrease in growth is accompanied by a reduction in motility (Suppl. Video 1 and 2), showing that the ablation of the channel has a negative effect in parasite's fitness.

TcMscS regulates parasites osmotic stress responses

To evaluate the role of TcMscS in cell volume regulation, we exposed the parasites to osmotic changes and followed the variations in absorbance over time, as an indicator of variations in cell volume. Under hypoosmotic conditions (Fig. 6A) TcMscS-KD and KO epimastigotes experienced a maximum change in volume of about 38% compared with 23-25% in the controls (Table 1, Peak and Fig. 6B). When we analyzed the rate of recovery between 200-400 s, no significant difference was observed in the slope values, except for TcMscS-KO that shown a slightly higher value. Nevertheless, KD and KO parasites do not regain their normal volume after 600 s, showing a remaining volume change of about 20% (Table 1, Final volume, Fig. 6C).

These results indicate that TcMscS, similar to other MscS channels, activates in order to compensate increases in cell volume and prevent excessive cell swelling. Seemingly, TcMscS-KD and KO parasites under hypoosmotic stress do not loose complete control of their volume, suggesting that TcMscS must act in conjunction with other mechanisms to orchestrate effective regulatory volume decrease responses.

Upon hyperosmotic stress (Fig. 6D), a similar phenotype was observed, with TcMscS-KD and TcMscS-KO parasite reducing their volume about 20%, compared with 12-15% in the controls (Table 2, Peak; Fig. 6E). As previously described (45), epimastigotes under hyperosmotic conditions do not regain normal volume, and parasites lacking TcMscS remained significantly more shrunk compared to controls (Fig. 6F), showing that TcMscS is required for normal cell volume homeostasis upon hyperosmotic stress. We evaluated whether TcMscS

localization changes upon osmotic stress and observed no differences in parasites under iso-, hypo- or hyperosmotic conditions at different time points (Fig. S6).

It should be noted that TcMscS-KD and KO epimastigotes under isosmotic conditions show a cell volume about 36-38% higher than normal when compared with WT and Cas9 controls (Fig. S6). This significant difference underscores the role of TcMscS in the regulation of cell volume under normotonic conditions.

In order to recapitulate the osmotic stress phenotype observed in TcMscS-KD and KO parasites, we evaluated the RVD responses of the parasites in the presence of channel blockers. Nifedipine, a known inhibitor of L-type calcium channels, had a small but significant effect, reducing the slope of recovery and the RVD at 700 s (Fig. S8 B, blue line). Gadolinium, a known inhibitor of mechanosensitive channels (46), had a dramatic effect (Fig. S8 A), inducing continuous cell swelling and bursting of the cells (Fig. S8 B, red line). Similar effect was observed even under isosmotic conditions (data not shown). These results are consistent with the blockade of compensatory mechanisms that maintain cell volume, but they must to be analyzed carefully since Gd^{+3} has low specificity and could be also targeting other channels and pumps.

TcMscS-KO impairs parasite differentiation and infectivity

To elucidate the role of TcMscS in *T. cruzi's* infectivity, we first evaluated the localization of the channel in metacyclic trypomastigotes (Fig. 7A). Similar to tissue-derived trypomastigotes, TcMscS is localized mostly in the CVC bladder of the metacyclic forms, with some labeling along the cell body, on the flagellar attachment zone region. The differentiation to metacyclic trypomastigotes *in vitro* is severely impaired in TcMscS-KO parasites, with a production of only 0.38% vs 6% obtained from WT epimastigotes after 72h of incubation in TAU media (Fig. 7B). We were able to infect mammalian cells with TcMscS-KO metacyclic trypomastigotes and obtained tissue culture derived trypomastigotes. The infective capacity of

these trypomastigotes was not affected at early time points post-infection (Fig. 7C, 6 h; Table 3) but showed a significant decrease in the production of intracellular amastigotes at 48 h post-infection (Fig. 7C and E; Table 3). These results suggest a defect in the capacity of the TcMscS-KO to replicate intracellularly. Quantification of extracellular trypomastigotes collected from the tissue culture supernatant also shown a significant decrease in the number of TcMscS-KO parasites able to successfully differentiate into bloodstream trypomastigotes and egress from the cells (Fig. 7D). At 6 dpi, TcMscS-KO produced a total amount of of 5.2 x 10^6 extracellular parasites, almost one order of magnitude lower than the amount produced by Cas9-scr strain and WT parasites (Table 4). These differences in the fitness of TcMscS-KO parasites suggest the participation of the channel at different stages of differentiation and host cell infection process.

Discussion

Propagation of *T. cruzi,* involving alternated passage through mammalian and insect hosts, imposes specific demands on adaptability, protective mechanisms and strong differentiation potential, driving massive cell remodeling. All these mechanisms require special components that are likely to be unique to these protozoans, whose identification and understanding may provide more pharmacological targets to be used in the fight against these parasites. The data presented above show that TcMscS, a MscS-like mechanosensitive channel found in *T. cruzi*, is required for proper osmoregulation and is required for growth and differentiation. The channel appears to play special roles of balancing osmotic and/or contractile forces in a stage and location-specific manner.

In protozoan parasites, only a handful of ion channels have been identified and characterized by direct electrophysiological approaches (47-49). Existing data support their physiological roles in pH and membrane potential maintenance(50, 51), Ca^{2+} homeostasis (52-54) and osmoregulation (8, 48), but in most cases the link between these functions and the

single molecule properties of the channels responsible for them has yet to be established. Here we provide the first molecular and functional study of mechanosensitive channels in trypanosomatids.

Expression in Δ7 *E. coli* spheroplasts provided us a clean experimental system to study activation by tension and single-channel properties of TcMscS. The linear non-rectifying conductance of the channel is approximately half of the conductance of EcMscS (40). Similar to other MscS-like channels, TcMscS has a slight selectivity towards anions, but the size of the pore appears be sufficient for permeation of small organic osmolytes. An activation midpoint near 12 mN/m determined in bacterial spheroplasts suggests that the channel becomes fully active at tensions approaching the lytic limit, and thus it fulfills the role of an emergency valve permitting equilibration of osmolytes. TcMscS activities recorded in a distant heterologous expression system strongly suggest that the channel is gated directly by tension in the lipid bilayer without the need for cytoskeleton or other Tc-specific components. The ramp responses of TcMscS populations indicate a slow closing rate that allows the channel to remain open for a longer period thus relieving the hypoosmotic stress more completely. This ensures that the tension has dropped considerably below the threshold for TcMscS and the channel will not be flickering between the open and closed states in response to small fluctuations in tension.

The homology model of TcMscS depicts the channel as a heptameric assembly (39) of 2-TM subunits with both N- and C- termini on the cytoplasmic side of the membrane. The N-terminal alpha-helical domain, which is analogous to TM1 of EcMscS but much shorter, is likely oriented parallel to the bilayer. The model emphasizes the conserved role of the transmembrane helix 3 (TM3) lining the pore, with a residue F64 (homologous to L109 in EcMscS) forming the main gate of the channel and a KD flexible motif below the gate analogous to either KD or QG found in bacterial homologs. The alignment with bacterial channel sequences also predicts a conserved beta domain, which may contain a hypothetical second

hydrophobic gate. The C-ends are modeled as unstructured flexible linkers terminating with a short alpha-helical bundle, resembling the C-terminus of MscL. This arrangement is likely acting as a pre-filter at the cytoplasmic entrance to the pore.

In *T. cruzi*, TcMscS shows a differential localization in the extracellular vs intracellular stages of the parasite. In epimastigotes, the channel has a defined intracellular localization in the bladder of the contractile vacuole and partially colocalizes with VAMP-7 and actin. There are no previous reports of actin associated to the bladder of the CV, but we have shown the presence of myosin heavy chains V1 and V2 (43) suggesting the presence of a contractile machinery that might contribute to the periodic contraction of the organelle, similar to what it has been described in *D. discoideum and Paramecium (55, 56)*. In tissue-derived bloodstream and *in vitro*-differentiated metacyclic trypomastigotes, in addition to the CVC localization, TcMscS is also detected along the cell body and the flagellar attachment zone, suggesting that the channel function could be related with sensing of the tension changes during flagellar beating.

The role of CVC in parasite's osmoregulation has been clearly established as responsible for the regulatory volume decrease upon hypoosmotic stress (8). Proteomic and functional analysis of the CVC has shown the presence of numerous proteins involved in volume compensation (43) but no sensor of the osmotic state has been identified. We propose that TcMscS is activated upon excessive filling of the bladder, similar to what has been proposed in other protists (9, 56, 57). If the normal exocytotic release of the bladder content fails to relieve pressure, the channel activation may release the CVC content back to the cytoplasm thus preserving the integrity of the CVC.

We should note that intracellular amastigotes develop and proliferate in a constant-osmolarity cytosolic environment. At this stage, the channel is not detected in the CVC bladder, but instead is distributed only on the periphery of the round cells, in the plasma membrane. When the amastigotes are released to the extracellular media by bursting of the host cells,

TcMscS remains localized in the plasma membrane indicating that the localization is developmentally regulated and independent of the ionic concentration in the media. Because amastigotes are nearly spherical, they have little membrane reserve for swelling and thus are much more vulnerable to osmotic downshock compared to elongated cells with a larger surface-to-volume ratio. Here, TcMscS might be playing a different role, protecting the parasites from a sudden drop in osmolarity and facilitating cell volume adjustments in the course of active cell reshaping during differentiation to trypomastigotes. TcMscS expression levels are clearly developmentally regulated, with higher levels in epimastigotes at the exponential phase of growth. Changes in expression and localization of the channel could be responding to stage-specific cues as well as external conditions, allowing the parasites to transition successfully through their developmental cycle. To test this hypothesis, we used CRISPR/Cas9 (58) to downregulate TcMscS in the parasites and produced two strains with similar characteristics but different level of phenotypic defects. Neither the mutation or the elimination of the gene resulted in a lethal phenotype, but both cell lines had a significant reduction in their extracellular and intracellular replication and were impaired in their ability to produce metacyclic and bloodstream trypomastigotes, thus, decreasing the infectivity of the parasites.

TcMscS knockout strains exhibited considerably reduced motility and loss of infectivity. This is consistent with recent studies showing that motility is necessary for virulence in *T. brucei* (59). In trypanosomatids, flagellar beating and motility are regulated by Ca^{2+} transients generated in a directional manner along the flagellum (60).The generation of Ca^{2+} waves linked to the activation of mechanosensitive channels has been demonstrated in Chlamydomonas (61), tubular kidney cells (62, 63), lung epithelial lining (64) and bone cells (21). In *T. brucei*, a putative Ca^{2+} channel has been shown to be essential for flagellar attachment and cell viability (65) suggesting that Ca^{2+} is required for normal function. It is possible that activation of TcMscS along the flagellar attachment zone modulates Ca^{2+} dynamics, affecting motility and infectivity of the parasites. Preliminary data indicates that TcMscS mutants have lower than normal

intracellular Ca^{2+} levels and slow Ca^{2+} responses upon addition of the channel blocker Gd^{+3} (not shown). Additionally, our RNAseq data show significant downregulation of FLAM3, kinesin and other flagellar proteins, which may explain the defect in motility observed in TcMscS-KO parasites (Suppl. videos 1 and 2).

Regarding the reduction of growth rates in TcMscS-KO parasites, it is not clear how *T. cruzi* regulates the size of the population. Recent studies show that intracellular amastigotes regulate their growth and metabolism in response to the host conditions (66, 67). MSCs channels are regulators of homeocrowding, a mechanism that allows bacteria to maintain a constant level of macromolecular excluded volume at the expense of accumulating or releasing small osmolytes and metabolites (68, 69). This may constitute a novel way of linking the host metabolism with the intracellular replication of the parasite and could explain some of the cell density-related stage transitions observed *in vivo* and *in vitro*.

As expected, the mutant parasites also showed a decrease ability to control the cell volume both under stress and normal conditions, confirming the role of TcMscS in osmotic homeostasis. The partial RVD observed in the knockout parasites suggest that other channels could be involved in the compensatory responses. This has been well documented in bacteria, where knockout of MscS and MscL are required to elicit a defect in osmoregulation. In *T. cruzi*, bioinformatic analysis shows the presence of genes encoding for putative Piezo-like (38) and TRP-like channels(70), bacterial-like mechanosensitive channels that could contribute to stretch-dependent responses in the parasites. Our preliminary RNAseq analysis of TcMscS-KO parasites do not show a significant change in the expression of those genes (data not shown). These results do not rule out the possibility of an increase in channel activity, independent of the expression level. It could also indicate the absence of interdependence of expression levels within this functional class of channels.

In summary, we have identified and characterized at the molecular level the first mechanosensitive channel in trypanosomatids. TcMscS plays a pleiotropic role in these

parasites, affecting the capacity of the cells to respond to osmotic stress, proliferate, move, remodel and infect host cells. Our work opens new avenues to explore the connection between signaling pathways implicated in the differentiation and host-parasite interaction. It could also unveil the relationship between sensing of external cues and the factors that drive stage development of protozoans in a host-specific manner.

Material and Methods

TcMscS sequence analysis

Predicted protein sequences for TcMscS CL Brener Esmeraldo-like (TcCLB.504171.40) and Non-Esmeraldo-like haplotyoe (TcCLB.509795.40) were compared with the putative sequences for *Trypanosoma brucei* (Tb427.10.9030) and *Leishmania major* (LmjF.36.5770) MscS-like channels. Multiple alignments were compared with sequences for *E. coli* (WP_000389819) and *H. pilory* (WP_000343449.1) MscS channels. All the analysis was performed in Clustal Omega (https://www.ebi.ac.uk/Tools/msa/clustalo/). Linear topology predictions were done comparing the transmembrane domain predictions of TopPred, TMpred and TMHMM 2.0 (https://www.expasy.org/tools/). Sequence similarity was analyzed using SIAS online tool (http://imed.med.ucm.es/Tools/sias.html). BLOSUM62, PAM250 and GONNET indexes were used to compare TcMscS and other MscS-like protein sequences.

Molecular simulation of TcMscS structure

Structural predictions were performed by six independent servers/predictors (I-TASSER, Robetta, Phyre2, SWISS-MODEL, IntFOLDTS, and RaptorX). Eight different structures of *E. coli* MscS (2oau, 2vv5, 4agf, 4hwa, 5aji) and its homologs from *T. tengcongensis* (3t9n TtMscS, 3udc chimera of TtMscS and EcMscS beta barrel), and from *H. pylori* (4hw9) were selected as templates based on automated analysis of sequence similarity and structural trends. All the monomeric predictions were assembled into heptamers using SymmDoc. After visual and

automated inspection of the models, comparison of the consensus trends, and filtering for matching the hydrophobicity pattern of the membrane, and absence of severe structural conflicts we have picked one of the models (produced by IntFOLD2 server) as the most likely draft for the closed state conformation of TcMscS. We have manually adjusted the C-terminal amphipathic helix (connected by long flexible linkers to the cytoplasmic beta domains) to form a coiled-coil barrel, similar to what was observed in the crystal structures of another type of bacterial mechanosensitive channel, MscL.

The whole assembly was embedded into pre-equilibrated POPC bilayer and refined in Molecular Dynamics simulations (CHARMM36 force field) using iterative relaxation (5 ns) / symmetry-driven simulated annealing (1 ns) protocol. The refined closed state model was taken as a starting point in search of the open state structure using MD simulations with Extrapolated Motion Protocol to explore the conformational space. Structural analysis of the produced 5400 structures revealed the most promising candidate for the open state, included in Fig. 1.

Electrophysiological recordings of TcMscS

For electrophysiological studies in *E. coli* giant spheroplasts we used a N-terminally 6-His tagged version of *TcMscS* cloned into the expression plasmid pQE80 (Qiagen) with restriction sites BamHI and HindIII. TcMscS was expressed in the MJF641 (aka Δ7) strain devoid of seven endogenous MS channel genes (71). The strain was a gift from Dr. Ian Booth (University of Aberdeen, UK). Competent MJF641 cells were transformed, selected overnight for transformants on plates with 100 μg/ml ampicillin, and use immediately for spheroplast preparation. 2-3 colonies were grown in LB + %1 glucose for 1.5-2 hours. Spheroplast preparation was done following standard protocols (72). Briefly, 3 ml of the colony-derived culture was transferred into 27 ml of LB containing 0.06 mg/ml cephalexin to block septation. After 1.5-2 hours of shaking in the presence of cephalexin, 1 mM IPTG was added to induce protein expression for 20 min. The filaments were transferred into a hypertonic buffer containing

1 M sucrose and subjected to digestion by lysozyme (0.2 mg/ml) in the presence of 5 mM EDTA resulting in spheres of 3-7 µm in diameter. The reaction was terminated by adding 20 mM Mg^{2+}. Spheroplasts were separated from the rest of the reaction mixture by sedimentation through a one-step sucrose gradient.

Recording conditions and protocols

Borosilicate glass (Drummond 2-000-100) pipets with tips 1-1.3 µm in diameter (bubble number 4.9-5.1) were used to form tight seals with the inner membrane. The tension-activated channel activities were recorded in excised inside-out patches. In most experiments the pipette and bath solution were symmetrical (200 mM KCl, 50 mM $MgCl_2$, 5 mM $CaCl_2$, 5 mM HEPES, pH 7.4). The bath solution was supplemented with 400 mM sucrose to osmotically balance the spheroplasts. An asymmetric configuration 425 mM /200 mM KCl (bath/pipette) was used to determine the channel's anion/cation selectivity. Traces were recorded using Clampex 10.3 software (MDS Analytical Technologies). Programmed mechanical stimuli were delivered using a modified high-speed pressure clamp apparatus (HSPC-1; ALA Scientific Instruments).

Cell culture

Wild-type Y-strain (WT) epimastigotes were cultured in Liver Infusion Tryptose medium (LIT) (68.44 mM NaCl, 5.36 mM KCl, 56.35 mM Na_2HPO_4, 0.2% glucose, 0.5% Trypticase, 0.5% Liver Infusion, Hemin 0.02% w/v) supplemented with 10% heat-inactivated fetal bovine serum (FBS-HI) (73). Epimastigotes transfected with pTREX constructs including overexpressing (TcMscS-OE), Cas9scr and TcMscS mutants (TcMscS-KD and TcMscS-KO) were cultured in LIT media supplemented with 10% FBS-HI and selection antibiotics (250 µg/mL of geneticin (G-418) and 15 µg/ml blasticidin) (58).

Tissue-derived bloodstream trypomastigotes and amastigotes were obtained as previously described (16). Human foreskin fibroblast (HFF) and HEK-293 cells were cultured in High

Glucose Dulbecco's Modified Eagles Media (HG-DMEM) supplemented with 100 units/mL of penicillin, 100 µg/mL of streptomycin, 0.2% of amphotericin B, and 10% FBS-HI, and incubated at 37 °C with 5 % CO2.

In Vitro Metacyclogenesis

Differentiation to metacyclic trypomastigote forms was induced under chemically defined conditions using triatomine artificial urine (TAU) medium as described (74). Epimastigote cultures were started at 1×10^6 cells/mL in LIT media supplemented with 10% FBS-HI. After 4 days, cells were collected by centrifugation at 1600 × g for 10 minutes, washed once in phosphate buffered saline solution (PBS) pH 7.4, resuspended in TAU media (190 mM NaCl, 17 mM KCl, 2 mM $MgCl_2$, 2 mM $CaCl_2$, 8 mM Na_2HPO_4, and 0.035% $NaHCO_3$) and incubated 2 hours at 28 °C. The supernatant was collected and resuspended in TAU with amino acids (TAU3AAG) (TAU with 10 mM L-proline, 50 mM sodium L-glutamate, 2 mM sodium L-aspartate, and 10 mM glucose). Cultures were incubated in TAU3AAG for up to 7 days at 28°C, collected by centrifugation resuspended in 5 mL of Dulbecco's Modified Eagles Media (DMEM) supplemented with 20% fresh FBS and incubated overnight at 37°C. In the presence of complement proteins from the serum only metacyclic trypomastigotes survive.

In vitro infection assays

HFF or HEK-293 cells were plated onto coverlips in 12 well plates (1,000 cells/well) and incubated in supplemented HG-DMEM overnight at 37°C with 5% CO_2. Infections were performed at a multiplicity of infection (MOI) of 25:1 with either WT, Cas9scr or TcMscS mutant trypomastigotes. After 6 hours, the cells were washed 3 times with Hank's media and fresh DMEM was added. Coverslips were fixed in 4% paraformaldehyde-PBS at 6, 24 and 48 h, stained with DAPI (5 µg/ml) and mounted in Fluoromont media for quantification of intracellular

parasites or processed for immunofluorescence. Immunofluorescence assays were performed to verify expression of Cas9-GFP and TcMscS in intracellular amastigote forms. Cells were incubated with primary anti-TcMscS (1:100) antibody and primary anti-GFP rabbit serum (Thermo Fisher Scientific, Inc.) (1:3,000) antibody, followed by secondary antibodies anti-Guinea Pig Alexa-594 (ThermoFisher Scientific) and anti-Rabbit Alexa-488, respectively. The cells were observed in an Olympus IX83 microscope and pictures were acquired and processed with CellSens Dimension software.

All infection quantifications were done in 4 coverslips per experiment, in 3 or more independent experiments. At least 100 host cells were quantified per coverslip. The number of host cells vs. parasites was compared by a two-way ANOVA.

Quantification of extracellular trypomastigotes

The amount of infective forms released from HEK-293 cells infected at a MOI of 25:1 was evaluated by collecting the supernatant of the cultures at days 4, 5 and 6 post-infection. To eliminate possible contamination with detached cells, the supernatant was first centrifuged at 300 x g for 5 minutes. The supernatant containing trypomastigotes was then centrifuged at 1,600 x g for 5 minutes and resuspended in 1 ml of DMEM. The cells were counted in a Z2 Beckman Coulter cell counter. All quantifications were done in triplicate for 3 independent experiments.

TcMscS cloning, expression and antibody generation

The complete ORF of *TcMscS* was amplified with primers 1 and 2 (Table S1) from total genomic DNA from Y strain epimastigotes, cloned into pCR™-Blunt II TOPO® vector (Invitrogen), and sub-cloned into the pQE80 bacterial expression vector with restriction sites BamHI and HindIII. Bacterial expression of *TcMscS* ORF in BL21 plysS was induced overnight at 37°C with 1 mM isopropyl β-D-1-thiogalactopyranoside (IPTG). Recombinantly expressed TcMscS protein was

extracted under denaturing conditions and purified with a nickel-agarose affinity column (Pierce). Polyclonal antibodies against the whole protein were obtained by guinea pig immunization, following standard protocols (Cocalico Biologicals Inc., Reamstown, PA).

Western-blot analysis

For western blot analysis, parasites were collected at 1,600 x *g* for 10 min, washed twice in PBS, pH 7.4, and resuspended in modified RIPA buffer (150 mM NaCl, 20 mM Tris-Cl pH 7.5, 1 mM EDTA, 1% SDS and 0.1% Triton X-100) containing protease inhibitor cocktail. Total homogenates were separated by SDS-PAGE, transferred onto nitrocellulose membranes and blocked overnight with 5% nonfat dry milk in PBS-0.1% Tween 20 (PBS-T). Blotting was done with anti-TcMscS (1:1,000) or anti- GFP (1: 5,000) for 1 h at room temperature. Secondary antibodies conjugated with horseradish peroxidase or fluorescent DyLight 680 or 800 (LI-COR, Inc., Lincoln, NE) were used when indicated. Membranes were stripped with 62.5 mM Tris-HCl, pH 6.8, 2% SDS, 1% β-mercaptoethanol at 50°C for 30 min, extensively washed in PBS-T and incubated with monoclonal α-tubulin (Sigma) (1:5,000) as a loading control.

Immunofluorescence analysis

Epimastigotes, bloodstream trypomastigotes and host cells containing intracellular amastigotes were fixed for 30 minutes in 4% paraformaldehyde. Fixed cells were attached to poly-L-lysine-treated glass coverslips for 10 minutes. Samples were permeabilized with 0.3 % Triton X-100 for 3 minutes, washed in 1x PBS three times and incubated in 50 mM NH4Cl for 30 minutes at room temperature. After blocking overnight at 4 °C in 3 % bovine serum albumin (BSA) solution, the cells were incubated with antibodies against TcMscS (1:500), GFP (1:3,000), actin (1;250), tubulin (1:500), SSP1 (1:250) or SSP4 (1:250) as indicated. Anti-SSP1 (# NR-50891) and anti-SSP4 (# NR050892) were obtained from BEI Resources, NIAID, NIH. The secondary antibodies were conjugated with Alexa- fluor 488 or 594 (1:3,000) (Thermo Fischer Scientific,

Inc., Waltham, MA). Coverslips were mounted with Fluoromount-G® (SouthernBiotech, Birmingham, AL) containing DAPI (5 µg/mL). To evaluate the localization of TcMscS under osmotic stress, epimastigotes exposed to hypo or hyper osmotic conditions were fixed at times 0, 2 and 5 minutes post-stress and processed for immunofluorescence analysis as indicated before. Immunofluorescence samples were imaged in an Olympus© IX83 inverted microscope system and processed with CellSense Olympus software. Alternatively, samples were imaged in an ELYRA S1 (SR-SIM) Super Resolution Microscope (Zeiss) and processed with ZEN 2011 software, kindly provided by the Biomedical Microscopy Core at the University of Georgia.

TcMscS mutant generation by CRISPR/Cas9

Two strategies were developed to generate TcMscS-KD and TcMscS-KO mutants using the CRISPR/Cas9 one-vector system (58). WT epimastigotes were transfected only with sgRNA/Cas9/pTREXn vector containing a sgRNA targeting *TcMscS*. Alternatively, the single vector containing TcMscS-sgRNA was co-transfected with a donor DNA to induce double strand break repair by homologous recombination, carrying a blasticidin resistance marker and 100 bp flanking regions of *TcMscS.* Three rotospacer adjacent motifs (PAM) sites within the *TcMscS* gene were identified and guide RNAs (sgRNA) were designed to specifically target the gene. To avoid off target effects, the protospacers were screened against the whole *T.* cruzi genome using ProtoMatch-V 1.0 kindly provided by Sebastian Lourido (75). The sgRNAs targeting *TcMscS* were amplified with forward primers listed in Table S1 (P7, 8 and 9) and reverse P10 using plasmid pUC_sgRNA as template (58). The amplicons were cloned into TOPO-Blunt vector and subcloned into sgRNA/Cas9/pTREXn vector. Successful cloning of TcMscS-sgRNAs was confirmed by sequencing. Two donor templates were constructed using the gene encoding blasticidin-S deaminase (Bsd) amplified from tdTomato/pTREX-b (58) and the ultramers indicated in Table 1 (P9-12). The first donor template contained 5' and 3'-UTR regions of *TcMscS* flanking the *Bsd* cassette *.* The second donor template had the *Bsd gene* flanked by

the last 100 bp of coding sequence of *TcMscS* and 100 bp of the 3'-UTR. Plasmid containing a scrambled sgRNA and Cas9 in a pTREXn vector were used as controls. To simplify the labeling the cell line expressing Cas9 and the scrambled sgRNA is labeled Cas9.

Cell transfections

Y-strain epimastigotes were grown for 4 days under standard conditions, collected at 1600 × *g* for 10 minutes, washed once with BAG, and resuspended in 100 µL of Human T Cell Nucleofector Solution (Lonza). 5×10^7 cells were mixed with 5 µg of each sgRNA plasmid with or without 5 µg of DNA donor and electroporated under the U-033 Amaxa Nucleofector protocol. Cells were allowed to recover overnight and appropriate antibiotics for selection (250 µg/mL G-418 and 15 µg/mL of blasticidin) were added.

TcMscS-GFP overexpression construct

The ORF of *TcMscS* was amplified without a stop codon from genomic DNA extracted from WT epimastigotes (76) and subcloned with EcoRI and HindIII subcloned into the pTREX-C-GFP (Addgene #: 62544). pTREX-C-GFP-TcMscS plasmid was verified by sequencing and transfected into WT epimastigotes as described above.

Genomic screening of transfectants

Total genomic DNA was extracted from WT, Cas9, TcMscS-KD and TcMscS-KO and analyzed by PCR to evaluate the presence of *TcMscS* (Table S1 P1-2) or the DNA donors (Table S1 P3-4 for blasticidin, P5-6 *TcMscS* downstream). GADPH amplification was used as a housekeeping gene for loading control (Table S1, P15-16).

Genomic DNA from epimastigotes was sequenced to confirm the deletion of a single nucleotide in the TcMscS-KD and insertion of the DNA donors in the TcMscS-KO.

TcMscS expression levels

TcMscS mRNA expression was assessed by RT-qPCR in the three life stages of the parasite as well as in WT, Cas9, TcMscS-KD and TcMscS-KO. Epimastigotes were collected during mid-log phase of growth, washed once with 1x PBS pH 7.4 and homogenized in TRI Reagent® at a density of $1x10^7$ parasites/ml. Total mRNA was extracted following the manufacturer protocol (Sigma-Aldrich, St. Louis, MO) followed by chloroform/ ethanol precipitation. mRNA was converted to cDNA using SuperScript® III First-Strand Synthesis System (ThermoFisher Scientific, Inc. Waltham, MA) with oligo-$dT_{(20)}$ primers. cDNA was analyzed by qPCR with Power SYBR Green PCR Master Mix (Applied Biosystems) and primers P1-P2 for *TcMscS.*

For trypomastigotes analysis, the parasites were collected by centrifugation from supernatants of infected HEK-293 cells at 5 days post-infection. Amastigotes were collected from HEK-293 cells at 3 days post-infections. The cells were detached with a cell scrapper and mechanically lysed. Host cell debris were eliminated by centrifugation at 300 x g for 5 min, and the supernatants containing the amastigotes were collected at 1,600 x g for 10 min. The pellets were inspected by microscopy to verify the absence of host cells. RNA extraction and cDNA synthesis were performed as indicated for epimastigotes.

All qPCR results were normalized against GAPDH as housekeeping gene (Table S1, P15-16) and indicated as $\Delta\Delta$Cq Mean $\pm$ SD of at least 3 independent experiments in triplicate.

Growth curves

Growth of epimastigotes was measured in TcMscS-KD, TcMscS-KO, WT and Cas9 control parasites starting at a concentration of $1\text{-}5 \times 10^6$ cells/mL in LIT media supplemented as previously described. The number of parasites was determined daily using a Z Series Coulter Counter (Beckman Coulter) The results are expressed as Mean $\pm$ SD of 3 independent experiments, in triplicate.

Osmotic stress assays

Epimastigotes at log phase of growth (3 days) were collected at 1,600 x *g* for 5 min, washed twice in PBS and resuspended in isosmotic buffer (64 mM NaCl, 4 mM KCl, 1.8 mM $CaCl_2$, 0.53 mM $MgCl_2$, 5.5 mM glucose, 150 mM D-mannitol, 5 mM Hepes-Na, pH 7.4, 282 mOsmol/L) at a cell density of 1 x 10^8/ml. Aliquots of 100 µL of parasites were placed in a 96-well plate in isosmotic buffer and relative cell volume changes after osmotic stress were measured by light scattering method(48).Briefly, pre-treatment readings of parasites in isosmotic buffer were taken for 3 minutes, followed by addition of 200 µL of hyposmotic buffer (64 mM NaCl, 4 mM KCl, 1.8 mM $CaCl_2$, 0.53 mM $MgCl_2$, 5.5 mM glucose, 5 mM HEPES-Na, pH 7.4) was added for a final osmolarity of 115 mOsmol/L. Alternatively, the cells were subjected to hyperosmotic stress with 200 µL of hyperosmotic buffer (64 mM NaCl, 4 mM KCl, 1.8 mM $CaCl_2$, 0.53 mM $MgCl_2$, 5.5 mM glucose, 500 mM D-mannitol, 5 mM HEPES-Na, pH 7.4). The absorbance at 550 nm was measured every 10 seconds for 12 minutes. The absorbance readings were normalized against the average from the first three minutes of pre-treatment. Normalized absorbance readings were then converted into a percent volume change using the following equation: $[(V_F - V_i)/V_F] \times 100$, where V_F is the absorbance value at the experimental time point and V_i is the initial absorbance value obtained at the same time point under isosmotic conditions.

The maximum volume change was calculated by peak function analysis between 150-250 sec. The final recovery volume was evaluated between 600-700 sec. The results are the Mean ± SE of 5 independent experiments in triplicate for all the cell lines.

Effect of ion channel blockers under osmotic stress

Epimastigotes osmotic responses upon hypoosmotic shock was evaluated in the presence of ion channel blockers. The hypoosmotic buffer containing the blockers was added to a final

osmolarity of 115 mOsmol/L and final concentrations of $GdCl_3$ (10 μM), Streptomycin (100 μM), Amiloride (1 μM), or Nifedipine (10 μM). Changes in cell volume were recorded and calculated as indicated before for osmotic stress experiments.

Live video microscopy under osmotic stress

WT and TcMscS mutant epimastigotes were loosely adhered to poly-L-lysine treated glass bottom coverslips under isosmotic conditions. After adherence, the epimastigotes were subjected to hyposmotic stress under the same conditions described above. Live video microscopy was taken under DIC illumination for 600 seconds in an Olympus© IX83 inverted microscope system.

Statistical analysis

All the experiments were performed at least 3 times with intra-experiment replicates. the results are presented as Mean ± SD or SE as indicated in the figure legend. Statistical significance was evaluated by one- or two-way ANOVA with ad-hoc Bonferroni post-test or Student t- test as indicated in the figures.

Acknowledgments

Dr. Roberto Docampo for his guidance and manuscript revisions, Stephen Vella and Dr. Myriam Hortua-Triana for assistance with super resolution imaging. Dr. Nikolas Nikolaidis kindly provided antibodies against actin.

This work was funded by the National Institute of Health NIAID grant R15AI122153 and American Heart Association grant 16GRNT30280014 to VJ, and scholarship from Cal State Fullerton MARC U*STAR Program grant 2T34GM008612-23 to JF.

References

1. Jimenez V (2014) Dealing with environmental challenges: mechanisms of adaptation in Trypanosoma cruzi. *Res Microbiol* 165(3):155-165.
2. Cowman AF, Healer J, Marapana D, & Marsh K (2016) Malaria: Biology and Disease. *Cell* 167(3):610-624.
3. Silvester E, McWilliam KR, & Matthews KR (2017) The Cytological Events and Molecular Control of Life Cycle Development of Trypanosoma brucei in the Mammalian Bloodstream. *Pathogens* 6(3).
4. Perez-Molina JA & Molina I (2018) Chagas disease. *Lancet* 391(10115):82-94.
5. Requena-Mendez A*, et al.* (2015) Prevalence of Chagas disease in Latin-American migrants living in Europe: a systematic review and meta-analysis. *PLoS Negl Trop Dis* 9(2):e0003540.
6. Bern C & Montgomery SP (2009) An estimate of the burden of Chagas disease in the United States. *Clin Infect Dis* 49(5):e52-54.
7. Kollien AH & Schaub GA (1998) Development of Trypanosoma cruzi after starvation and feeding of the vector - a review. *The Tokai journal of experimental and clinical medicine* 23(6):335-340.
8. Rohloff P & Docampo R (2008) A contractile vacuole complex is involved in osmoregulation in Trypanosoma cruzi. *Exp Parasitol* 118(1):17-24.
9. Docampo R, Jimenez V, Lander N, Li ZH, & Niyogi S (2013) New insights into roles of acidocalcisomes and contractile vacuole complex in osmoregulation in protists. *Int Rev Cell Mol Biol* 305:69-113.
10. Girard-Dias W, Alcantara CL, Cunha-e-Silva N, de Souza W, & Miranda K (2012) On the ultrastructural organization of Trypanosoma cruzi using cryopreparation methods and electron tomography. *Histochem Cell Biol* 138(6):821-831.
11. Allen RD & Naitoh Y (2002) Osmoregulation and contractile vacuoles of protozoa. *Int Rev Cytol* 215:351-394.
12. Niyogi S, Mucci J, Campetella O, & Docampo R (2014) Rab11 regulates trafficking of trans-sialidase to the plasma membrane through the contractile vacuole complex of Trypanosoma cruzi. *PLoS Pathog* 10(6):e1004224.
13. Montalvetti A, Rohloff P, & Docampo R (2004) A functional aquaporin co-localizes with the vacuolar proton pyrophosphatase to acidocalcisomes and the contractile vacuole complex of Trypanosoma cruzi. *The Journal of biological chemistry* 279(37):38673-38682.
14. Rohloff P, Montalvetti A, & Docampo R (2004) Acidocalcisomes and the contractile vacuole complex are involved in osmoregulation in Trypanosoma cruzi. *The Journal of biological chemistry* 279(50):52270-52281.
15. Furuya T, Kashuba C, Docampo R, & Moreno SN (2000) A novel phosphatidylinositol-phospholipase C of Trypanosoma cruzi that is lipid modified and activated during trypomastigote to amastigote differentiation. *The Journal of biological chemistry* 275(9):6428-6438.
16. Moreno SN, Silva J, Vercesi AE, & Docampo R (1994) Cytosolic-free calcium elevation in Trypanosoma cruzi is required for cell invasion. *J Exp Med* 180(4):1535-1540.
17. Cox CD, Bavi N, & Martinac B (2017) Bacterial Mechanosensors. *Annual review of physiology*.
18. Arnadottir J & Chalfie M (2010) Eukaryotic mechanosensitive channels. *Annual review of biophysics* 39:111-137.
19. Alfieri RR & Petronini PG (2007) Hyperosmotic stress response: comparison with other cellular stresses. *Pflugers Archiv : European journal of physiology* 454(2):173-185.
20. Miura S, Sato K, Kato-Negishi M, Teshima T, & Takeuchi S (2015) Fluid shear triggers microvilli formation via mechanosensitive activation of TRPV6. *Nature communications* 6:8871.
21. Corrigan MA*, et al.* (2018) TRPV4-mediates oscillatory fluid shear mechanotransduction in mesenchymal stem cells in part via the primary cilium. *Sci Rep* 8(1):3824.

22. Li J*, et al.* (2014) Piezo1 integration of vascular architecture with physiological force. *Nature* 515:279.
23. Siryaporn A, Kuchma SL, O'Toole GA, & Gitai Z (2014) Surface attachment induces Pseudomonas aeruginosa virulence. *Proceedings of the National Academy of Sciences of the United States of America* 111(47):16860-16865.
24. O'Loughlin CT*, et al.* (2013) A quorum-sensing inhibitor blocks Pseudomonas aeruginosa virulence and biofilm formation. *Proceedings of the National Academy of Sciences of the United States of America* 110(44):17981-17986.
25. Thomen P*, et al.* (2017) Bacterial biofilm under flow: First a physical struggle to stay, then a matter of breathing. *PloS one* 12(4):e0175197.
26. Sukharev SI, Blount P, Martinac B, Blattner FR, & Kung C (1994) A large-conductance mechanosensitive channel in E. coli encoded by mscL alone. *Nature* 368(6468):265-268.
27. Martinac B, Buechner M, Delcour AH, Adler J, & Kung C (1987) Pressure-sensitive ion channel in Escherichia coli. *Proceedings of the National Academy of Sciences of the United States of America* 84(8):2297-2301.
28. Levina N*, et al.* (1999) Protection of Escherichia coli cells against extreme turgor by activation of MscS and MscL mechanosensitive channels: identification of genes required for MscS activity. *The EMBO Journal* 18(7):1730-1737.
29. Kloda A & Martinac B (2001) Molecular identification of a mechanosensitive channel in archaea. *Biophysical journal* 80(1):229-240.
30. Kumamoto CA (2008) Molecular mechanisms of mechanosensing and their roles in fungal contact sensing. *Nat Rev Microbiol* 6(9):667-673.
31. Yoshimura K (1998) Mechanosensitive channels in the cell body of Chlamydomonas. *J Membr Biol* 166(2):149-155.
32. Nakayama Y, Fujiu K, Sokabe M, & Yoshimura K (2007) Molecular and electrophysiological characterization of a mechanosensitive channel expressed in the chloroplasts of Chlamydomonas. *Proceedings of the National Academy of Sciences of the United States of America* 104(14):5883-5888.
33. Peyronnet R, Tran D, Girault T, & Frachisse JM (2014) Mechanosensitive channels: feeling tension in a world under pressure. *Frontiers in plant science* 5:558.
34. Palmer CP*, et al.* (2001) A TRP homolog in Saccharomyces cerevisiae forms an intracellular Ca(2+)-permeable channel in the yeast vacuolar membrane. *Proceedings of the National Academy of Sciences of the United States of America* 98(14):7801-7805.
35. Lee CP*, et al.* (2016) MSL1 is a mechanosensitive ion channel that dissipates mitochondrial membrane potential and maintains redox homeostasis in mitochondria during abiotic stress. *The Plant journal : for cell and molecular biology* 88(5):809-825.
36. Peyronnet R, Haswell ES, Barbier-Brygoo H, & Frachisse JM (2008) AtMSL9 and AtMSL10: Sensors of plasma membrane tension in Arabidopsis roots. *Plant signaling & behavior* 3(9):726-729.
37. Haswell ES & Meyerowitz EM (2006) MscS-like proteins control plastid size and shape in Arabidopsis thaliana. *Curr Biol* 16(1):1-11.
38. Prole DL & Taylor CW (2013) Identification and analysis of putative homologues of mechanosensitive channels in pathogenic protozoa. *PloS one* 8(6):e66068.
39. Bass RB, Strop P, Barclay M, & Rees DC (2002) Crystal structure of Escherichia coli MscS, a voltage-modulated and mechanosensitive channel. *Science (New York, N.Y.)* 298(5598):1582-1587.
40. Sukharev S (2002) Purification of the small mechanosensitive channel of Escherichia coli (MscS): the subunit structure, conduction, and gating characteristics in liposomes. *Biophysical journal* 83(1):290-298.

41. Belyy V, Kamaraju K, Akitake B, Anishkin A, & Sukharev S (2010) Adaptive behavior of bacterial mechanosensitive channels is coupled to membrane mechanics. *The Journal of general physiology* 135(6):641-652.
42. Chiang CS, Anishkin A, & Sukharev S (2004) Gating of the large mechanosensitive channel in situ: estimation of the spatial scale of the transition from channel population responses. *Biophysical journal* 86(5):2846-2861.
43. Ulrich PN*, et al.* (2011) Identification of contractile vacuole proteins in Trypanosoma cruzi. *PloS one* 6(3):e18013.
44. Niyogi S*, et al.* (2015) Rab32 is essential for maintaining functional acidocalcisomes, and for growth and infectivity of Trypanosoma cruzi. *J Cell Sci* 128(12):2363-2373.
45. Li ZH*, et al.* (2011) Hyperosmotic stress induces aquaporin-dependent cell shrinkage, polyphosphate synthesis, amino acid accumulation, and global gene expression changes in Trypanosoma cruzi. *The Journal of biological chemistry* 286(51):43959-43971.
46. Ermakov YA, Kamaraju K, Sengupta K, & Sukharev S (2010) Gadolinium ions block mechanosensitive channels by altering the packing and lateral pressure of anionic lipids. *Biophysical journal* 98(6):1018-1027.
47. Jimenez V, Henriquez M, Galanti N, & Riquelme G (2011) Electrophysiological characterization of potassium conductive pathways in Trypanosoma cruzi. *J Cell Biochem* 112(4):1093-1102.
48. Jimenez V & Docampo R (2012) Molecular and electrophysiological characterization of a novel cation channel of Trypanosoma cruzi. *PLoS Pathog* 8(6):e1002750.
49. Steinmann ME, Schmidt RS, Bütikofer P, Mäser P, & Sigel E (2017) TbIRK is a signature sequence free potassium channel from Trypanosoma brucei locating to acidocalcisomes. *Scientific Reports* 7(1):656.
50. Van Der Heyden N & Docampo R (2002) Proton and sodium pumps regulate the plasma membrane potential of different stages of Trypanosoma cruzi. *Molecular and biochemical parasitology* 120(1):127-139.
51. Van der Heyden N & Docampo R (2002) Significant differences between procyclic and bloodstream forms of Trypanosoma brucei in the maintenance of their plasma membrane potential. *J Eukaryot Microbiol* 49(5):407-413.
52. Pace DA, McKnight CA, Liu J, Jimenez V, & Moreno SN (2014) Calcium entry in Toxoplasma gondii and its enhancing effect of invasion-linked traits. *The Journal of biological chemistry* 289(28):19637-19647.
53. Chiurillo MA*, et al.* (2017) Different Roles of Mitochondrial Calcium Uniporter Complex Subunits in Growth and Infectivity of Trypanosoma cruzi. *MBio* 8(3).
54. Lander N, Chiurillo MA, Storey M, Vercesi AE, & Docampo R (2016) CRISPR/Cas9-mediated endogenous C-terminal Tagging of Trypanosoma cruzi Genes Reveals the Acidocalcisome Localization of the Inositol 1,4,5-Trisphosphate Receptor. *The Journal of biological chemistry* 291(49):25505-25515.
55. Plattner H (2013) Contractile vacuole complex--its expanding protein inventory. *Int Rev Cell Mol Biol* 306:371-416.
56. Tominaga T, Allen R, & y (1998) Electrophysiology of the in situ contractile vacuole complex of Paramecium reveals its membrane dynamics and electrogenic site during osmoregulatory activity. *J Exp Biol* 201(3):451-460.
57. Tani T, Allen RD, & Naitoh Y (2000) Periodic tension development in the membrane of the in vitro contractile vacuole of Paramecium multimicronucleatum: modification by bisection, fusion and suction. *J Exp Biol* 203(Pt 2):239-251.
58. Lander N, Li ZH, Niyogi S, & Docampo R (2015) CRISPR/Cas9-Induced Disruption of Paraflagellar Rod Protein 1 and 2 Genes in Trypanosoma cruzi Reveals Their Role in Flagellar Attachment. *MBio* 6(4).

59. Shimogawa MM*, et al.* (2018) Parasite motility is critical for virulence of African trypanosomes. *Sci Rep* 8(1):9122.
60. Edwards BFL*, et al.* (2018) Direction of flagellum beat propagation is controlled by proximal/distal outer dynein arm asymmetry. *Proceedings of the National Academy of Sciences of the United States of America* 115(31):E7341-e7350.
61. Collingridge P, Brownlee C, & Wheeler Glen L (2013) Compartmentalized Calcium Signaling in Cilia Regulates Intraflagellar Transport. *Current Biology* 23(22):2311-2318.
62. Nauli SM*, et al.* (2008) Endothelial cilia are fluid shear sensors that regulate calcium signaling and nitric oxide production through polycystin-1. *Circulation* 117(9):1161-1171.
63. Wu L, Gao X, Brown RC, Heller S, & O'Neil RG (2007) Dual role of the TRPV4 channel as a sensor of flow and osmolality in renal epithelial cells. *Am J Physiol Renal Physiol* 293(5):F1699-1713.
64. Schmid A & Salathe M (2011) Ciliary beat co-ordination by calcium. *Biology of the cell* 103(4):159-169.
65. Shimogawa MM*, et al.* (2015) Cell Surface Proteomics Provides Insight into Stage-Specific Remodeling of the Host-Parasite Interface in Trypanosoma brucei. *Molecular & cellular proteomics : MCP* 14(7):1977-1988.
66. Dumoulin PC & Burleigh BA (2018) Stress-Induced Proliferation and Cell Cycle Plasticity of Intracellular Trypanosoma cruzi Amastigotes. *MBio* 9(4).
67. Gazos-Lopes F, Martin JL, Dumoulin PC, & Burleigh BA (2017) Host triacylglycerols shape the lipidome of intracellular trypanosomes and modulate their growth. *PLoS Pathog* 13(12):e1006800.
68. Rowe I, Anishkin A, Kamaraju K, Yoshimura K, & Sukharev S (2014) The cytoplasmic cage domain of the mechanosensitive channel MscS is a sensor of macromolecular crowding. *The Journal of general physiology* 143(5):543-557.
69. van den Berg J, Boersma AJ, & Poolman B (2017) Microorganisms maintain crowding homeostasis. *Nat Rev Microbiol* 15(5):309-318.
70. Cruz-Bustos T, Moreno SNJ, & Docampo R (2018) Detection of Weakly Expressed Trypanosoma cruzi Membrane Proteins Using High-Performance Probes. *J Eukaryot Microbiol* 65(5):722-728.
71. Edwards MD*, et al.* (2012) Characterization of three novel mechanosensitive channel activities in Escherichia coli. *Channels (Austin, Tex.)* 6(4):272-281.
72. Delcour AH, Martinac B, Adler J, & Kung C (1989) Modified reconstitution method used in patch-clamp studies of Escherichia coli ion channels. *Biophysical journal* 56(3):631-636.
73. Bone GJ & Steinert M (1956) Isotopes incorporated in the nucleic acids of Trypanosoma mega. *Nature* 178(4528):308-309.
74. Contreras VT, Salles JM, Thomas N, Morel CM, & Goldenberg S (1985) In vitro differentiation of Trypanosoma cruzi under chemically defined conditions. *Molecular and biochemical parasitology* 16(3):315-327.
75. Sidik SM, Hackett CG, Tran F, Westwood NJ, & Lourido S (2014) Efficient genome engineering of Toxoplasma gondii using CRISPR/Cas9. *PloS one* 9(6):e100450.
76. Lahiri DK & Nurnberger JI, Jr. (1991) A rapid non-enzymatic method for the preparation of HMW DNA from blood for RFLP studies. *Nucleic Acids Res* 19(19):5444.

Figure legends

Figure 1. Sequence alignment and predictions of TcMscS structure by homology to EcMscS. A. Partial protein sequence alignment of four MscS-type channels from *T. cruzi T. cruzi* Esmeraldo-like (TcCLB.504171.40) and non-Esmeraldo-like (TcCLB.509795.40) haplotypes of the CL Brener reference strain, *T. brucei* (Tb427.10.9030) and *L. major* (LmjF.36.5770), with two bacterial MscS channels from *E. coli* (WP_000389819) and *H. pilory* (WP_000343449.1). The position of the transmembrane domains TM1, TM2 and TM3 are underlined, the position of the putative gate residues are indicated by red arrows, conserved residues forming the hinges of TM3 are indicated with asterisks. The full alignment can be found in supplemental Figure S1. **B**. Arrangements of transmembrane helices in the crystal structure of EcMscS (PDB ID 2OAU) and in the proposed homology model of TcMscS that was equilibrated and refined in simulations with all-atom POPC bilayer. Only the N-terminal helix (red), TM2 (gold), TM3 (green), and beta-domains of the cytoplasmic cage (cyan) are shown. The full homology TcMscS model in the closed and open states is presented in Figure S2 (supplement).

Figure 2. Electrophysiological properties of TcMscS. A. Single-channel currents at positive and negative pipette voltages **B.** Current-to-voltage relationships measured in symmetric (200 mM/200 mM KCl, black symbols, n=11) and asymmetric conditions (425mM/200 mM KCl, red symbols, n=4). The theoretical reversal potential for Cl^- and K^+ (grey arrows) and the experimental reversal potential measured for TcMscS (red arrow) are indicated. **C-E.** Examples of traces recorded with identical 1-s linear ramps on three separate patches bearing 11, 2 and 3 active channels at +30 mV (**C,D**) or -30 mV pipette potential (**E**). **F.** Multiple ramp responses of TcMscS were normalized to the current at saturating pressure and converted to dose-response curves. The aggregated TcMscS curve (black symbols, n=11) is compared with EcMscS dose-response curves (blue symbols, n=54). The inset in panel F shows the same dose-response curves plotted as log (Po/Pc) and fitted with the Boltzmann equation. **G, H.** TcMscS closing rate

in an 11-channel and 15-channel patches to an asymmetric (G) and symmetric (H) pressure ramp.

Figure 3. Localization and expression of TcMscS in *T. cruzi*. Immunolocalization of TcMscS (red) with specific polyclonal antibodies in epimastigotes **(A)**, trypomastigotes **(B)** and intracellular amastigotes **(C).** The right panels correspond to images of the same life stages obtained by super-resolution microscopy. Cellular structures are indicated as CV (contractile vacuole), K (kinetoplast) and N (nucleus). DNA was DAPI stained. Bar sizes: A = 5 µm; B and C = 5 µm. **D.** Expression of TcMscS in different life stages of the parasite, quantified by RT-qPCR. Trypomastigotes (Tryp) and amastigotes (Amast) were obtained from HEK-293 cells. Epimastigotes were analyzed at 4 days (Epis Exp) and 10 days of growth (Epis Stat). The values are indicated as ΔΔCq respect to the expression in trypomastigotes and normalized against GAPDH as housekeeping gene. The values are Mean ± SEM of 3 independent experiments in triplicate (* $p = 0.006$, # $p = 0.009$). **E.** Western blot analysis of TcMscS in trypomastigotes (T), amastigotes (A) and epimastigotes (E). Purified recombinant protein (R) was used as positive control. The whole cell lysates were probed with polyclonal antibodies against TcMscS and monoclonal anti-tubulin was used as loading control.

Figure 4. TcMscS targeting by CRISPR/Cas9 produced a knockdown effect. A. Partial alignment of TcMscS nucleotide sequencing (top panel) and predicted protein (bottom panel) obtained from wild-type epimastigotes CL Brener and Y strains, parasites expressing a scrambled sgRNA and Cas9 and those in which TcMscS specific sgRNA2 was transfected (TcMcsS-KD). A single nucleotide deletion in position 178 results in a shift in the ORF (black arrow) and a premature stop codon (red arrow). **B.** Growth curve of epimastigotes WT (black line), Cas9 (red line) and TcMscS-KD (blue line). Mean ± SEM of 3 independent experiments in triplicate (** $p<0.01$). **C.** RT-qPCR quantifying the expression of TcMscS in epimastigotes control (Cas9) vs TcMscS-KD. The values are indicated as ΔΔCq respect to the expression in

WT epimastigotes and normalized against GAPDH as housekeeping gene. All the samples were collected from parasites at 4 days of growth. The values are Mean ± SEM of 3 independent experiments in triplicate (# *p = 0.040*). **D.** Immunofluorescence analysis of TcMscS (red) in epimastigotes Y strain (WT), Cas9 and TcMscS-KD. The expression of Cas9 was detected with anti-GFP antibodies. Nuclei and kinetoplasts were DAPI stained. The position of the contractile vacuole is indicated with yellow arrows. Bar size= 5 µm.

Figure 5. Phenotypic characterization of TcMscS KO. A. Schematic representation of *TcMcS* gene targeting by CRISPR/Cas9. A double strand DNA cut was induced at position +185 and repaired by homologous recombination with construct containing the *Bsd gene*. The primers used for screening are listed in Table S1. **B.** gDNA screening of TcMscS KO epimastigotes by PCR. Negative controls (C) without DNA are in lane 1 for all reactions. The ORF for *TcMscS* was amplified in WT and Cas9 controls but absent in TcMscS KO parasites. The correct insertion of the blasticidin cassette (BSD) was verified by amplification with primers annealing in ORF and the 3'UTR. GAPDH was used as a housekeeping gene for loading control. **C.** Growth curve of epimastigotes WT (black line), Cas9 (red line), TcMscS KD (blue line) and TcMscS KO (green line). All the experiments were started at $1x10^6$/ ml cells and counted daily. The values are Mean ± SEM of 3 independent experiments in triplicate (*, ** $p<0.01$). **D.** RT-qPCR quantifying the expression of TcMscS in epimastigotes control (Cas9) vs TcMscS-KO. The values are indicated as ΔΔCq respect to the expression in WT epimastigotes and normalized against GAPDH as housekeeping gene. All the samples were collected from parasites at 4 days of growth. The values are Mean ± SEM of 3 independent experiments in triplicate (# *p = 0.0001*). **E.** Immunofluorescence analysis of TcMscS (red) in epimastigotes Y strain (WT), TcMscS-KO. Nuclei and kinetoplasts were DAPI stained. The position of the contractile vacuole is indicated with yellow arrows. Bar size= 2 µm.

Figure 6. Osmotic stress responses in TcMscS mutants. A. Regulatory volume decreases in epimastigotes. Cells suspended in isosmotic buffer recorded for 120 sec and diluted with to a final osmolarity of 115 mOsm/L under constant ionic conditions. Relative changes in cell volume were monitored by determining absorbance at 550 nm over time, in WT (black), Cas9 (red), TcMscS-KD (blue) and TcMscS-KO (green). The absorbance values were normalized by the initial volume under isosmotic conditions and expressed as percentage of volume change. **B.** Analysis of the maximum volume change under hypoosmotic conditions. The peak area was calculated between 150-250 sec for all the experiments. **C.** Final volume recovery calculated between 600-700 sec. **D.** Volume decrease in epimastigotes after hyperosmotic shock. After 3 min under isosmotic conditions, cells were placed under hyperosmotic stress at 650 mOsm/L. Volume changes were monitored and calculated as explained in **A.** Peak analysis **(E)** and final volumes were calculated at the same times that in **B** and **C.** The values for A-F are mean ± SEM of 5 independent experiments in triplicate ($p< 0.01$). Statistical analysis details are listed in Table 1 and 2. **G.** Representative immunofluorescence images of WT and TcMscS-KO epimastigotes at 2 min post hypo-osmotic stress. TcMscS (red) was detected with specific polyclonal antibodies against the channel. Nuclei and kinetoplasts were DAPI stained. Yellow arrows indicate the presence of cells with abnormal morphology, observed in the TcMscS-KO strain. Bar size= 2 µm.

Figure 7. Infectivity defects in TcMscS mutants. A. Representative immunofluorescence images showing the localization of TcMscS in metacyclic trypomastigotes labeled with anti-TcMscS antibodies (red). The position of the contractile vacuole is indicated by yellow arrows. Nuclei and kinetoplasts were DAPI stained. Bar size= 2 µm. **B.** Percentage of metacyclic forms obtained *in vitro* from WT and TcMscS-KO parasites incubated for 72 h in TAU 3AAG media. Values are mean ± SEM of 4 independent experiments (* $p= 0.039$). **C.** Quantification of intracellular amastigotes at 6 and 48 h post infection. HEK 293 cells were infected at a MOI of

25:1 with trypomastigotes WT (black), Cas9 (red), TcMscS-KD (blue) or TcMscS-KO (green). No significant differences were observed at 6 hpi. In contrast, at 48 h, TcMscS mutants show a significant decrease in intracellular amastigotes). Values are mean ± SEM of 5 independent experiments in triplicate (*p= 0.006; # p= 0.00008). **D.** Quantification of extracellular trypomastigotes released from infected HEK293 cells after 4 days of infection. Cells were infected at a MOI of 25:1 with WT (black), Cas9 (red) or TcMscS-KO (green) trypomastigotes and extracellular parasites were collected daily for counting. Values are mean ± SEM of 4 independent experiments (**p= 0.0037). **E.** Representative images of HEK293 cells infected with Cas9 (Cas9), TcMscS-KD or TcMscS-KO parasites. TcMscS was detected with specific antibodies (red), Cas9 was labeled with anti-GFP, nuclei and kinetoplasts were DAPI stained. Bar size= 10 μm.

A

```
TcruziEsm   ----------------------------------------MKRFFNRFYLDTG---IIADP
TcruziNonE  ----------------------------------------MKRFFNRFYLDTG---IIADP
Tbrucei     ----------------------------------------MKRFFDKLYHTTG---FIVDP
LmjF        ----------------------------------------MKRFFSSLYEGTG---IIKDP
Ecoli       MEDLNVVDSINGAGSWLVANQALLLSYAVNIVAALAIIIVGLIIARMISNAVNRLMISRK
Hpylori     ---------MDEIKTLLVDFFPQAKHFGIILIKAVIVFCIGFYFSFFLQKKT--MKFLSK
                                        TM1

TcruziEsm   SQRSLASRVSAFLVQGAVAFSLLGTIG---VDTSPLIAAAGVTGATIGFACKDFGTNFVA
TcruziNonE  SQRSLASRVSALLVQGAVAFSLLGTIG---VDTSPLIAAAGVTGATIGFACKDFGTNFVA
Tbrucei     SQRSVASHVSSLLLQGSIAFSLLGTIG---VDTSPLVAAAGVIGATAGFACKDFGANFIA
LmjF        GQRSIASRVTVLAVEGVAVFTVLGTLG---VDTSPLIAAAGVTGATIGFACKDFGANFVA
Ecoli       IDATVADFLSALVRYGIIAFTLIAALGRVGVQTASVIAVLGAAGLAVGLALQGSLSNLAA
Hpylori     KDEILANFVAQVTFILILIITTIIALSTLGVQTTSIITVLGTVGIAVALALKDYLSSIAG
                                                          *
                TM2                     TM3                gate   hinge 1

TcruziEsm   SIVLSGQQSIRTGNLVCIGTGLNVVKGKVVDWDTRYLYLRSSEGHLLHVPN-NMVLNSVV
TcruziNonE  SIVLSGQQSLRTGNQVCIGTGLNVVKGKVVDWDTRYLYLRSSEGHLLHVPN-NMVLNSVV
Tbrucei     SIVLSSQPSLRTGNRISIGTGAGAVKGEVVDWDTRYLYLRTSEGHLLHVPN-SMILTSIV
LmjF        SIALSGQRALRTGNKVSIGVGPNIVSGTVVDWDTRYIYLRNEERAVVCVPN-NVVLNSVV
Ecoli       GVLLVMFRPFRAGEYVDLGG----VAGTVLSVQIFSTTMRTADGKIIVIPNGKIIAGNII
Hpylori     GIILIILHPFKKGDIIEISG----LEGKVEALDFFNTSLRLHDGRLAVLPNRSVANSNII
            *
hinge 2                 beta domain
```

B

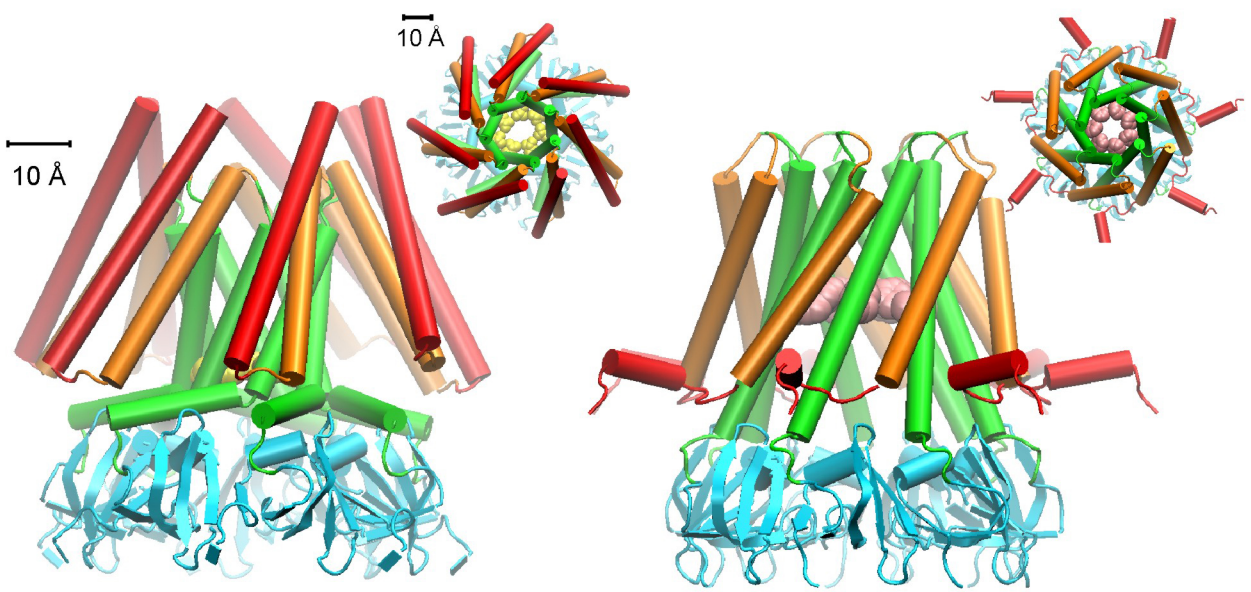

Fig. 1

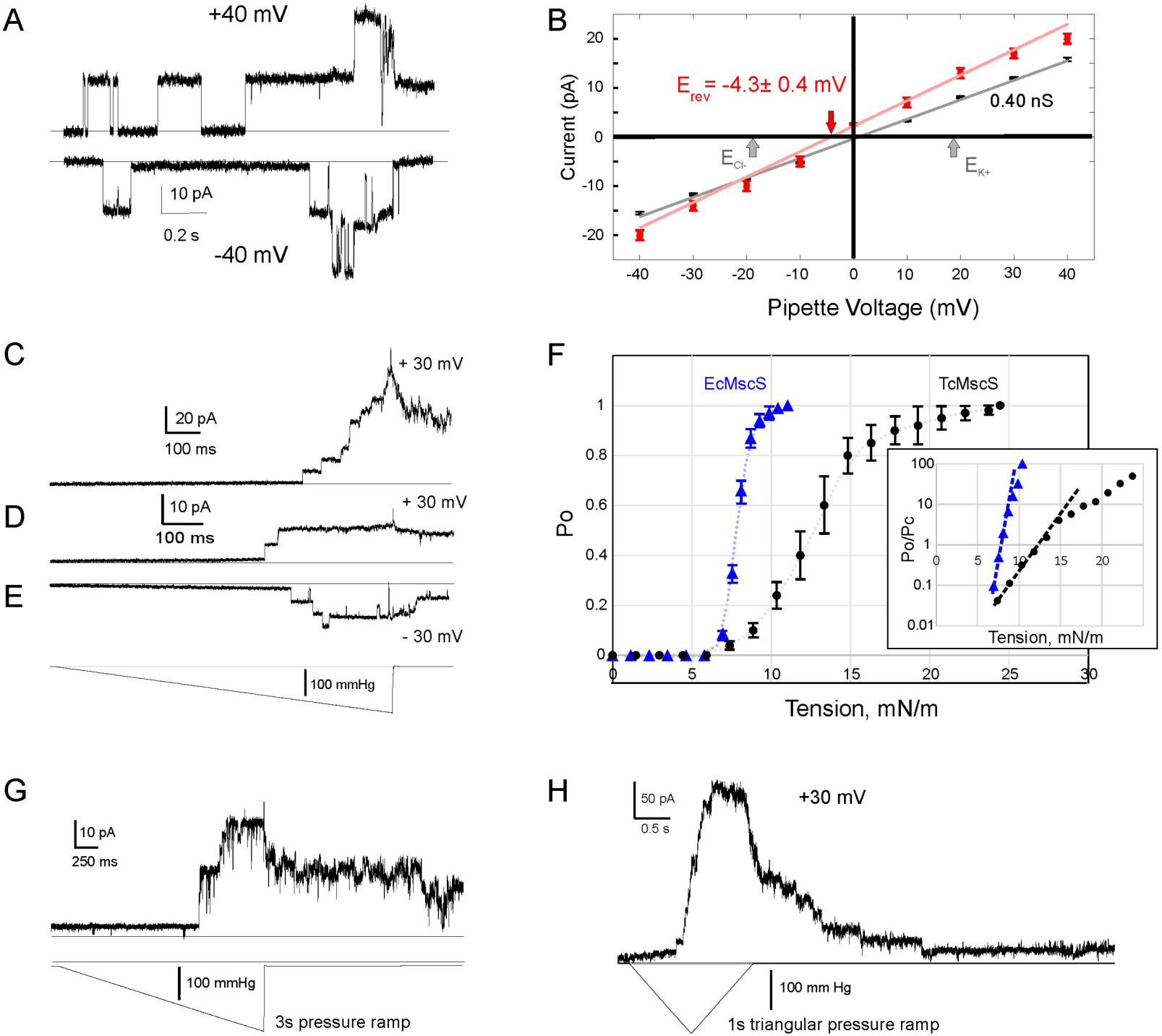
A
+40 mV
10 pA
0.2 s
-40 mV
B
E_{rev} = -4.3± 0.4 mV
0.40 nS
E_{Cl-}
E_{K+}
Current (pA)
Pipette Voltage (mV)
C
+ 30 mV
20 pA
100 ms
D
10 pA
100 ms
+ 30 mV
E
- 30 mV
100 mmHg
F
EcMscS
TcMscS
Po
Tension, mN/m
Po/Pc
Tension, mN/m
G
10 pA
250 ms
100 mmHg
3s pressure ramp
H
50 pA
0.5 s
+30 mV
100 mm Hg
1s triangular pressure ramp

Fig. 2

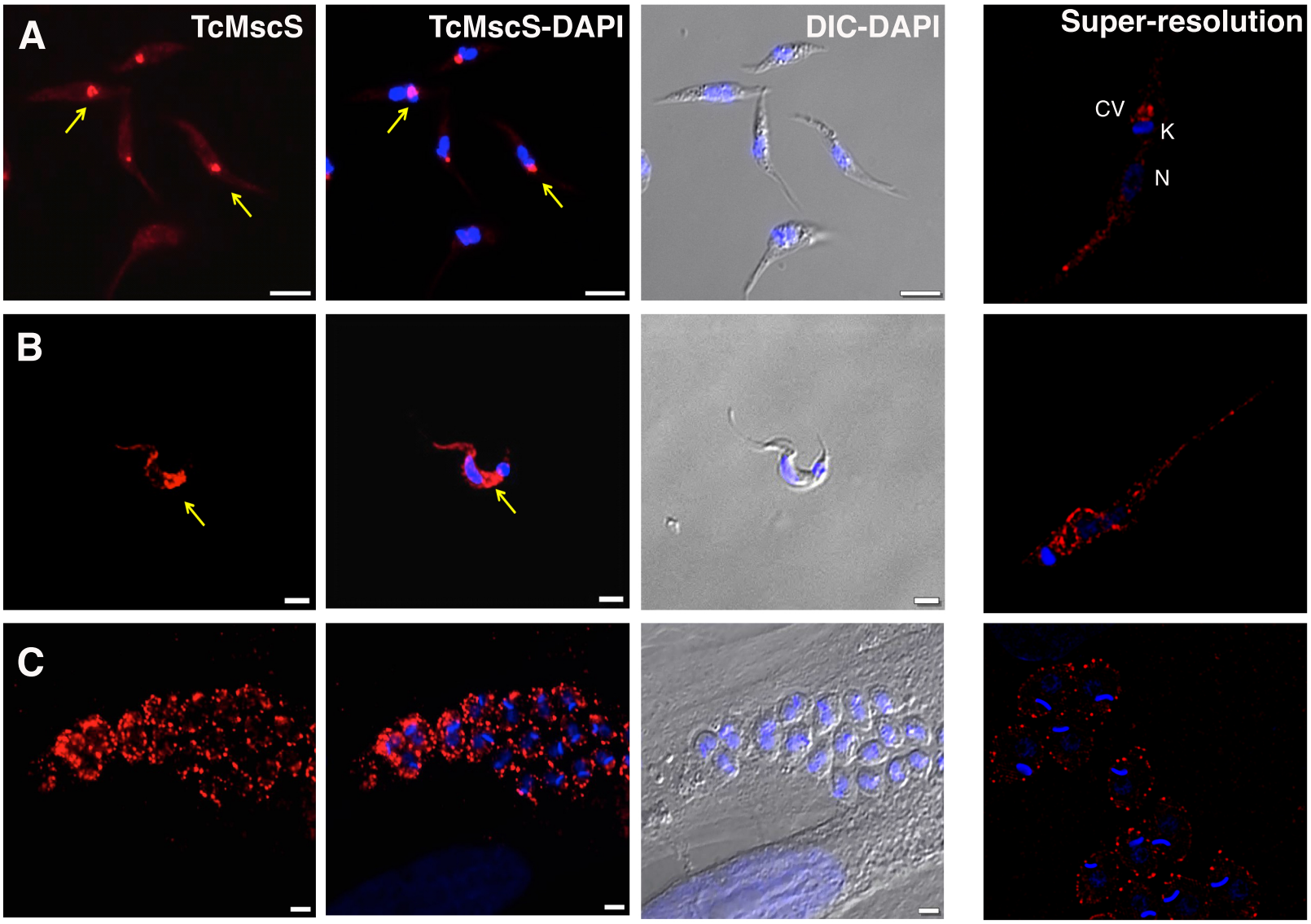
A
TcMscS
TcMscS-DAPI
DIC-DAPI
Super-resolution
CV
K
N
B
C

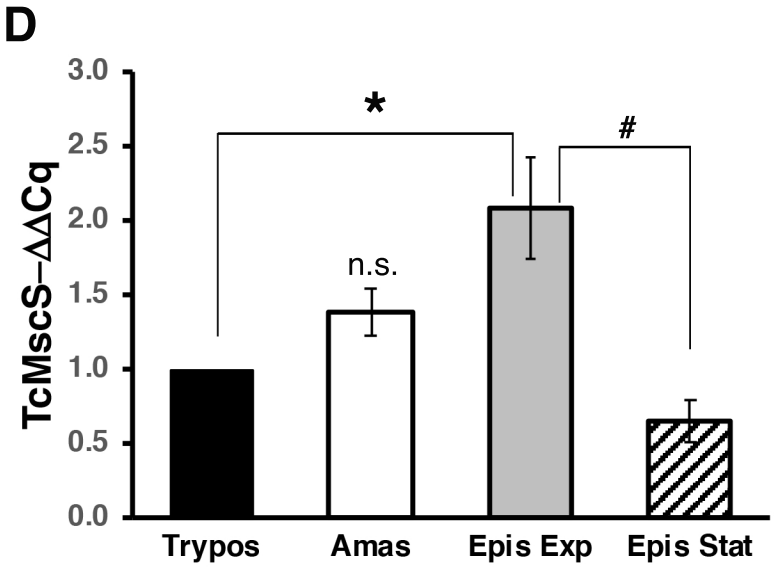
D
TcMscS–ΔΔCq
3.0
2.5
2.0
1.5
1.0
0.5
0.0
*
#
n.s.
Trypos
Amas
Epis Exp
Epis Stat

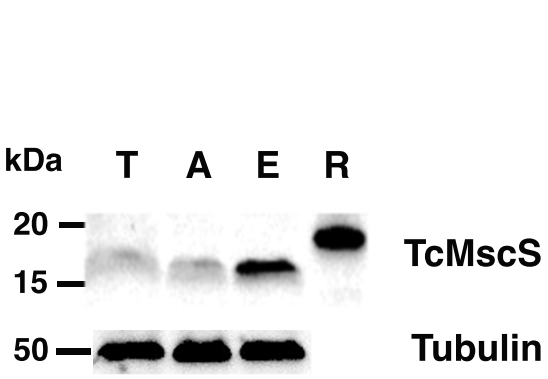
E
kDa
T
A
E
R
20
15
50
TcMscS
Tubulin

Fig. 3

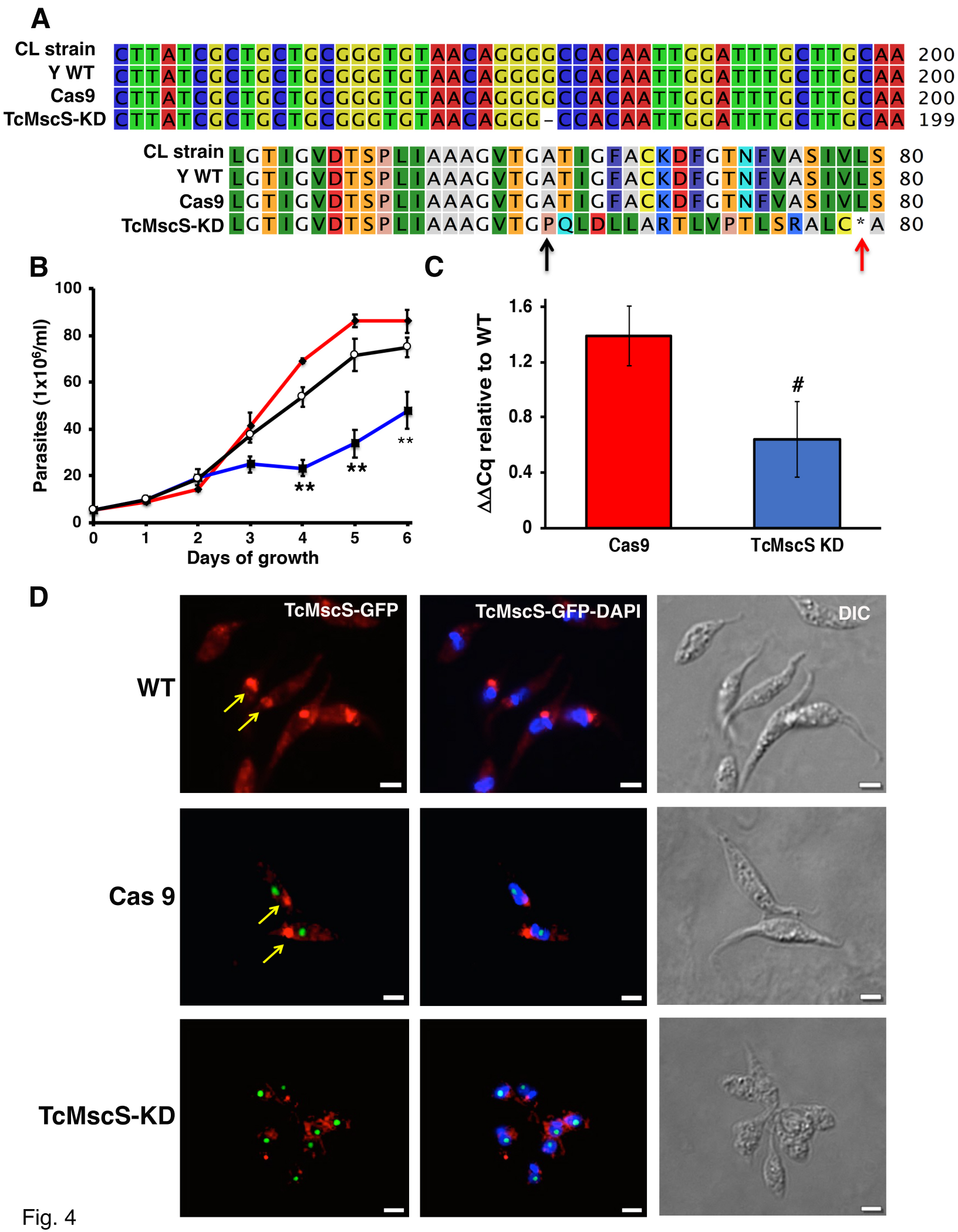
A
CL strain
Y WT
Cas9
TcMscS-KD
200
199
80
B
Parasites (1x10^6/ml)
Days of growth
C
ΔΔCq relative to WT
Cas9
TcMscS KD
#
D
TcMscS-GFP
TcMscS-GFP-DAPI
DIC
WT
Cas 9
TcMscS-KD

Fig. 4

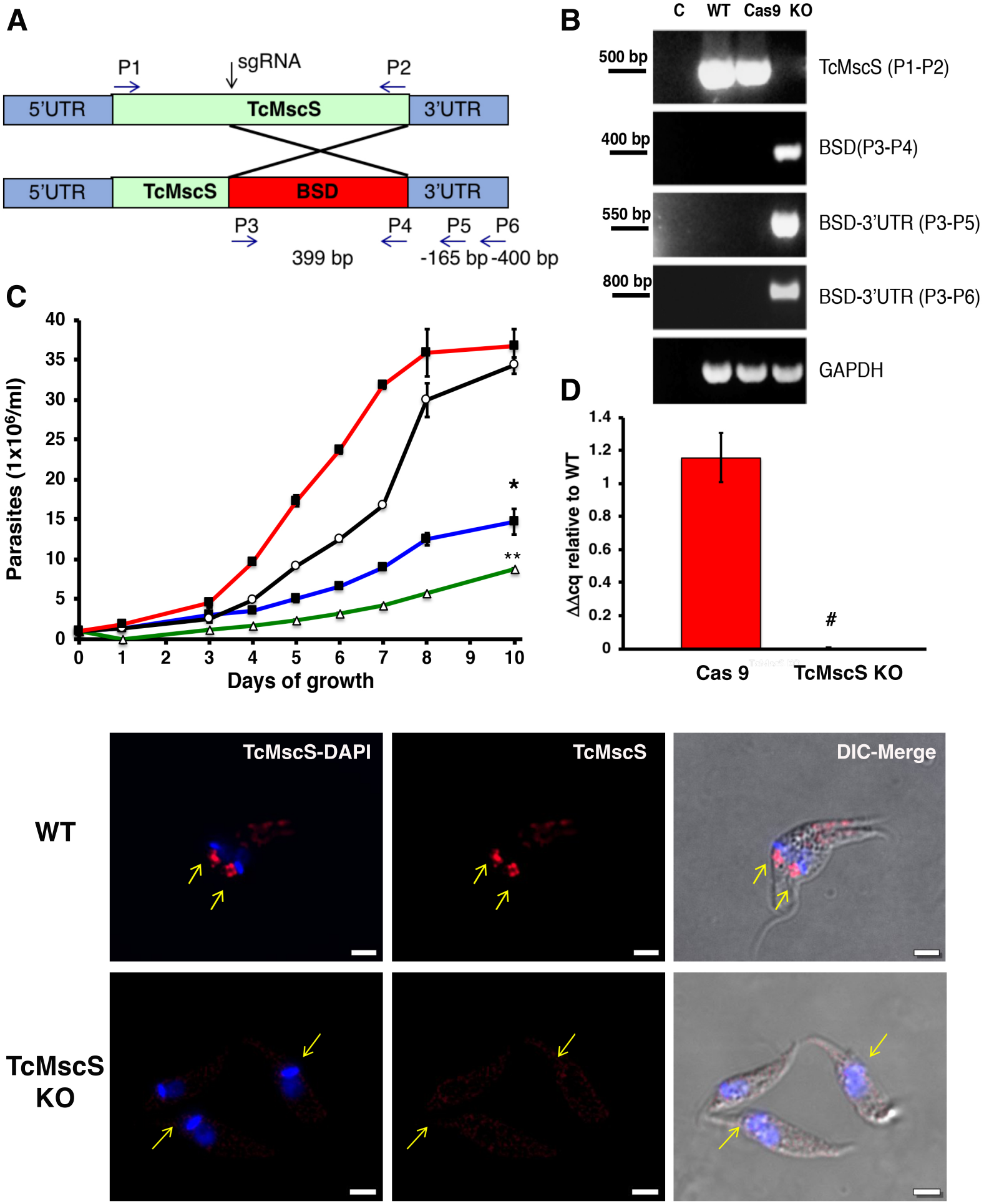
A
P1
sgRNA
P2
5'UTR
TcMscS
3'UTR
5'UTR
TcMscS
BSD
3'UTR
P3
P4
P5
P6
399 bp
-165 bp
-400 bp
B
C
WT
Cas9
KO
500 bp
TcMscS (P1-P2)
400 bp
BSD(P3-P4)
550 bp
BSD-3'UTR (P3-P5)
800 bp
BSD-3'UTR (P3-P6)
GAPDH
C
Parasites (1x10⁶/ml)
Days of growth
*
**
D
ΔΔcq relative to WT
#
Cas 9
TcMscS KO
TcMscS-DAPI
TcMscS
DIC-Merge
WT
TcMscS KO

Fig. 5

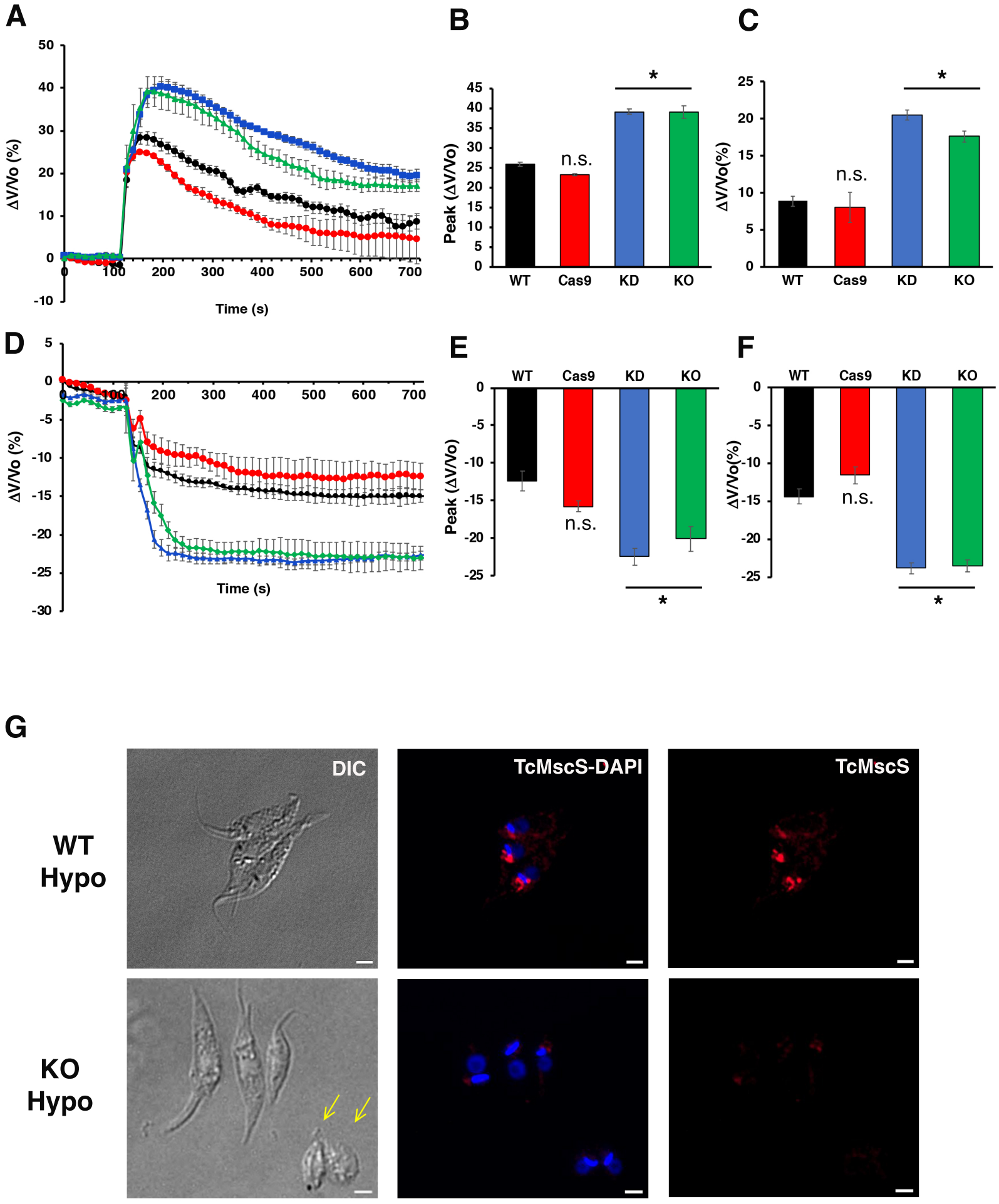
A
ΔV/Vo (%)
Time (s)
B
Peak (ΔV/Vo)
n.s.
*
WT
Cas9
KD
KO
C
ΔV/Vo(%)
n.s.
*
D
ΔV/Vo (%)
Time (s)
E
Peak (ΔV/Vo)
n.s.
*
F
ΔV/Vo(%)
n.s.
*
G
WT Hypo
KO Hypo
DIC
TcMscS-DAPI
TcMscS

Fig. 6

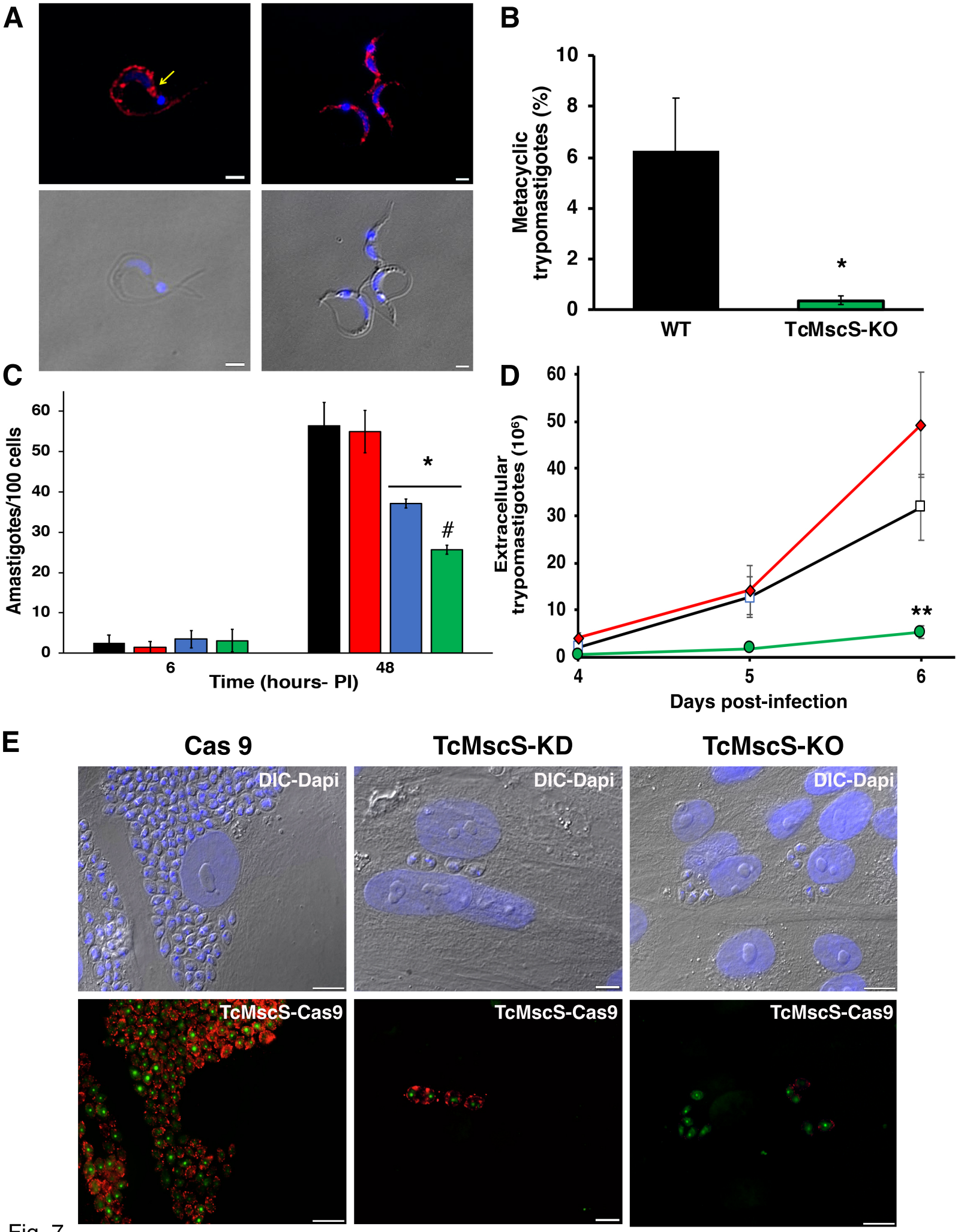
A
B
Metacyclic trypomastigotes (%)
10
8
6
4
2
0
*
WT
TcMscS-KO
C
Amastigotes/100 cells
60
50
40
30
20
10
0
*
#
6
48
Time (hours- PI)
D
Extracellular trypomastigotes (10⁶)
60
50
40
30
20
10
0
**
4
5
6
Days post-infection
E
Cas 9
TcMscS-KD
TcMscS-KO
DIC-Dapi
DIC-Dapi
DIC-Dapi
TcMscS-Cas9
TcMscS-Cas9
TcMscS-Cas9

Fig. 7

Table 1: Changes in cell volume upon hypoosmotic stress

	WT	Cas9	TcMscS-KD	TcMscS-KO
Peak (%)	25.83±0.52	23.08±0.23	39.10±0.63*	38.96±1.64*
p-value		0.575	$2.43E^{-09}$	$8.65E^{-05}$
Recovery slope	-0.0360±0.0029	-0.0327±0.0057	-0.0471±0.0031	-0.0685±0.002*
p-value		0.629	0.025	$7.3E^{-06}$
Final volume	8.86±0.71	7.99±2.05	20.48±0.65*	17.60±0.68*
p-value		0.7099	$2.96E^{-07}$	$4.95E^{-06}$

For all the conditions values are Mean±SE of n=5- p values were calculated based on one-way ANOVA analysis with Bonferroni post-test. Differences were considered significant when $p<0.01$(*).

Table 2: Changes in cell volume upon hyperosmotic stress

	WT	Cas9	TcMscS-KD	TcMscS-KO
Peak (%)	-12.41±1.36	-15.78±0.74	-22.43±1.12*	-20.10±1.59*
p-value		0.0055	0.0002	0.0043
Final volume	-14.38±0.93	-11.59±1.08	-23.84±0.71*	-23.56±0.82*
p-value		0.087	$4.27E^{-05}$	$7.99E^{-05}$

For all the conditions values are Mean±SE of n=5. p values were calculated based on one-way ANOVA analysis with Bonferroni post-test. Differences were considered significant when $p<0.01$(*).

Table 3: Quantification of intracellular amastigotes

Amas/100 cells	WT	Cas9	TcMscS-KD	TcMscS-KO
Average 6 h-pi	2.49±0.90	1.41±0.65	3.46±0.96	3.09±1.26
p-value		0.36	0.48	0.71
Average 48 h-pi	56.43±5.73	54.96±5.20	37.12±1.17*	25.64±1.06*
p-value		0.85	0.029	0.006

For all the conditions values are Mean±SE of n=5. p values were calculated based on one-way ANOVA analysis with Bonferroni post-test. Differences were considered significant when $p<0.05$(*).

Table 4: Quantification of extracellular trypomastigotes

Trypomastigotes (10^6)	WT	Cas9	TcMscS-KO
4 dpi	2.11±0.74	4.04±1.09	0.41±0.03
5 dpi	12.6±4.34	14.2±5.19	1.83±0.48
6 dpi	31.8±6.91	49.3±11.2	5.22±1.27*
p-value (6 dpi)		0.24	0.003

For all the conditions values are Mean±SE of n=4. p values were calculated based on one-way ANOVA analysis with Bonferroni post-test. Differences were considered significant when $p<0.05$(*).